ALEPH 90 - 66
PHYS 90 - 40
E.Lançon et al.
April 27,1990

PHOTONS IN HADRONIC EVENTS

E.Lançon, P. Perez, F. Perrier

Saclay

Abstract

Photons in hadronic events are studied using data collected in 1989. Problems with the data reconstruction and inadequacies of the Monte – Carlo simulation are discussed. Preliminary results on photon identification and π^0 inclusive production are presented. A search for prompt photons has been performed. Comparing the number of prompt photons with the expectation from final state radiation leads to a measurement of the u to d – type quark ratio in Z decays.

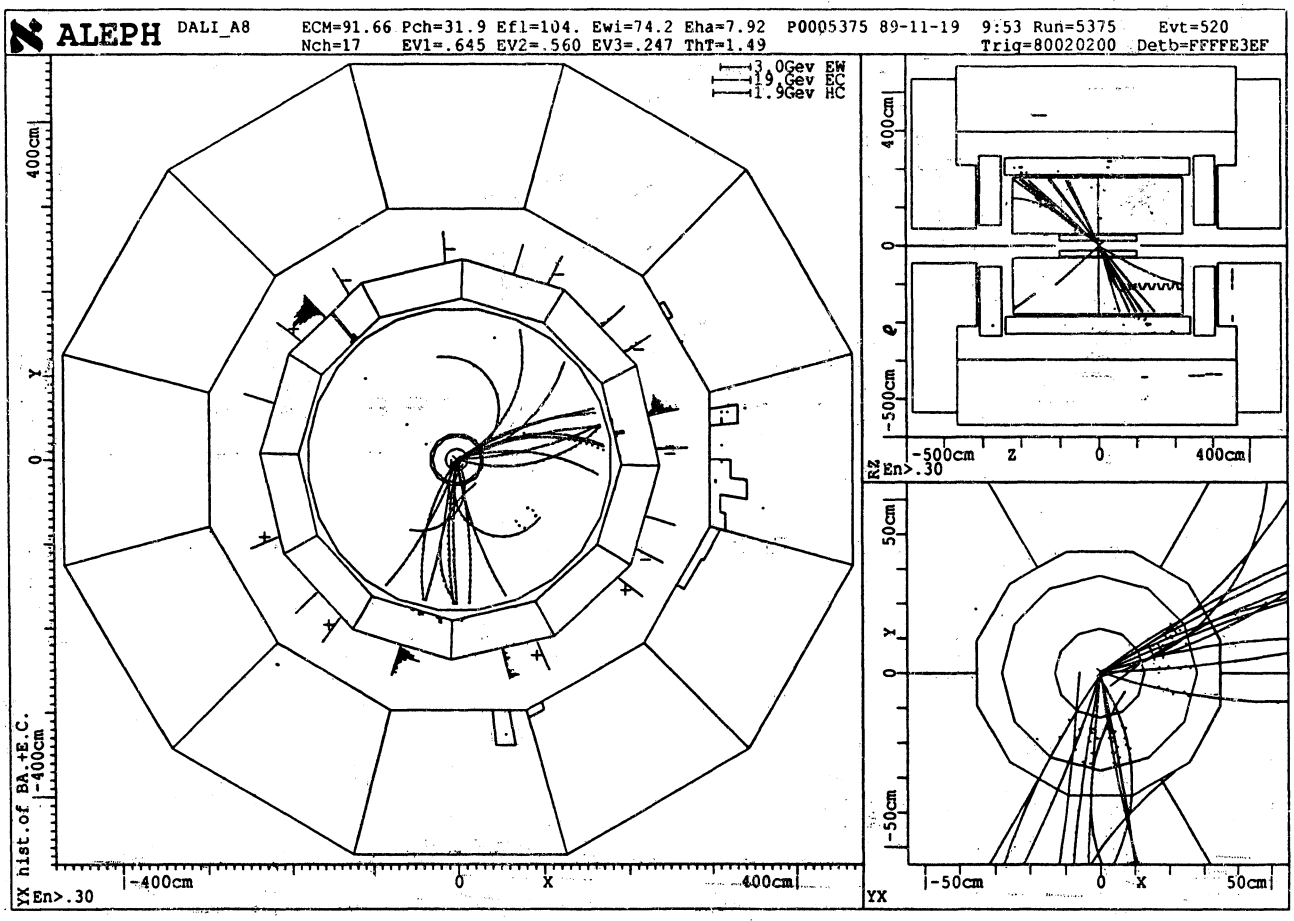

Figure 1: A hadronic event with a 28 GeV isolated photon.

Contents

Contents

Figures

Tables

1. INTRODUCTION

The purpose of this work is to study the behaviour in the ECAL barrel of the photons produced in hadronic events and to derive the physics of the production mechanisms for these photons.

Two kinds of photons produced in hadronic events will be distinguished. The *prompt* photons come from the pointlike e^+e^- interaction. They can be produced by initial or final state radiation, or by some new physics. All photons produced in subsequent decays or interactions with matter are called *non−prompt*.

On Figure 2 on page 2, the energy distribution of photons in the barrel region is shown separately for various sources, as given by the DYMU3 generator interfaced with LUND6.3. Photons from π^0 dominate at low energies while the spectrum of final state radiation photons has a slower decrease with energy and dominates above 30 GeV. Photons from initial state radiation are a negligible contribution in the barrel region. Photons coming from electron or positron bremstrahlung in the detector are not included in this figure. Above 10 GeV, their contribution amounts to 0.5% of the π^0 contribution and is therefore negligible.

In the first part of this note the photon identification in ALEPH will be discussed in some details. In the second part the low energy photons will be studied and the number of π^0's will be extracted from the data. Finally, high energy photons will be studied and a search for hard prompt photons will be performed.

1.1 Data Sample

1.1.1 Hadronic event selection

The data used are from 89, i.e POT reprocessed as of January 1990, with a selection on runs according to the *good runs* from SCANBOOK.

Hadronic events are selected with the following cuts:

- At least 5 "good" charged tracks, where a "good" track is defined as a TPC/ITC reconstructed track with $|d_0| \leq 1cm$, $|z_0| \leq 10cm$, $|\cos\theta| \leq 0.95$, at least 4 hits in the TPC, and momentum $\leq 200GeV$.

- The sum of the "good" track energies is larger than 10% of the center of mass energy ($E_{charged} \geq 0.1\sqrt{s}$)

- ECAL banks (PECO, PEST, ETDI) exist

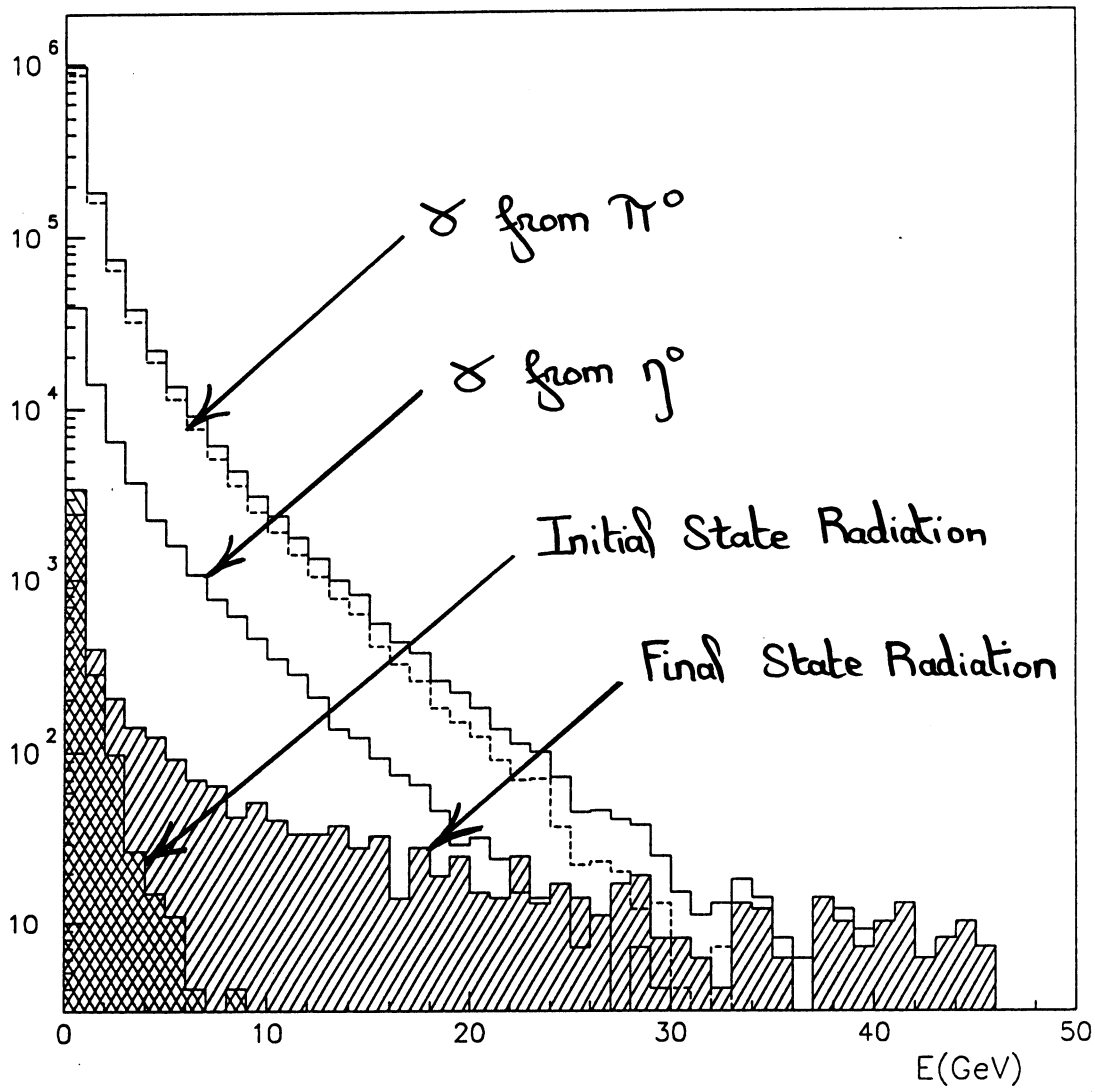

Figure 2: Energy distribution of photons in the barrel. Determined from DYMU3 generator. Detector simulation is not included.

This selects 25.640 events from the POT.

1.1.2 Monte − Carlo events

The Monte − Carlo simulation considered in this note is a production of 25000 $Q\bar{Q}$ events with HVFL01/DYMU02 (with final state radiation implemented correctly) at $\sqrt{s}$= 91.2 GeV , and GALEPH 237/JULIA 233. A total of 24366 events pass the previous selection.

2. Photon Identification

2.1 General overview of the ECAL

The electromagnetic calorimeter of ALEPH is a sandwidch of 45 lead sheets and proportional tubes. The barrel part consists of 12 modules. Each module covers 30° in ϕ and consists of $32(\phi)\times128(\theta)$ projective towers (granularity 1°×1°). Each tower is divided in three stacks, corresponding to a sampling of $\approx 4X_0$, $9X_0$ and $9X_0$. In addition, the energy profile in the 45 sampling planes is available for every module (wire readout).

2.2 Single Particle Studies

To study the ECAL response to photons and π^0, single particles (γ and π^0) of different energies have been generated in the barrel region with GALEPH and then reconstructed through JULIA. Particles result in clusters which are stored in the PECO bank. Photons are expected to have a small lateral extension and small energy deposition in stack 3.

- *NUMBER OF CLUSTERS*

Clusters are made with adjacent storeys above 30 MeV, and at least one storey above 90 MeV is required. A single photon interacting in the calorimeter may result in one or zero cluster, this is a consequence of the clustering. Low energy photons are often not reconstructed. Figure 3 on page 4 shows the percentage of photons resulting in zero or one cluster in the barrel as a function of the initial particle energy. Above 500 MeV one photon produces one cluster in more than 97% of the cases, at 300 MeV this percentage if 80 %.

- *LONGITUDINAL AND LATERAL PROFILE*

Owing to the excellent transverse granularity of the calorimeter (tower size ≈ 30×30 mm^2), a simple and discriminant variable can be defined to study the lateral profile of a cluster. This variable called F_4 is the fraction of energy deposited in the four leading towers around the most energetic one, in a cluster. For the longitudinal profile, it is impossible in general to make use of the information from the 45 wire planes, since several clusters of different energies are present in a given module. However, one can use the three stacks of the towers.

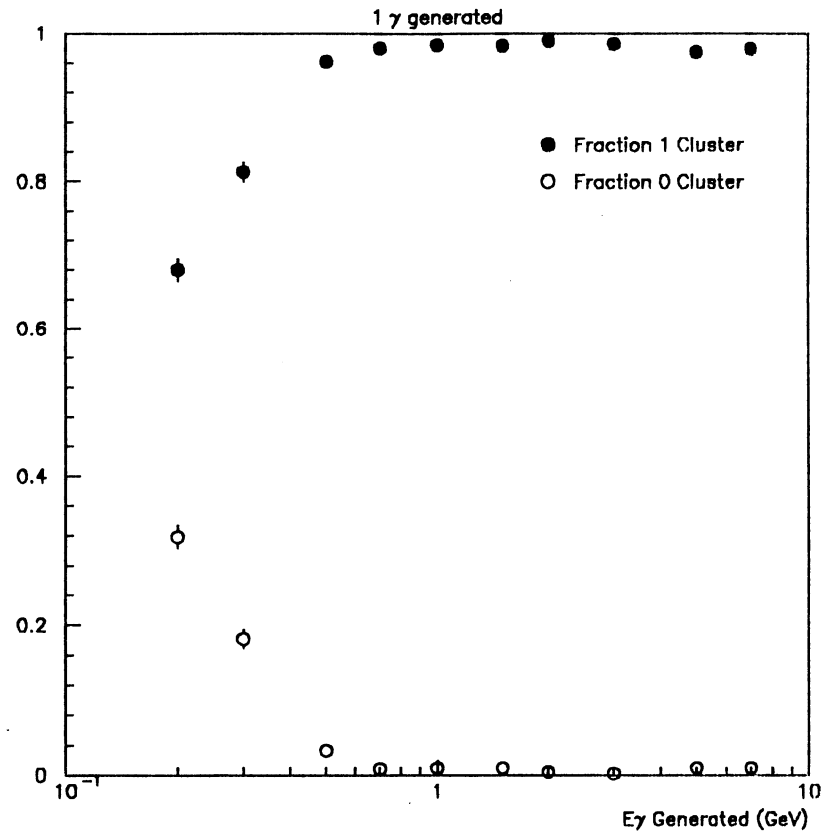

Figure 3: Fraction of photons resulting in one or zero clusters. Determined on single Monte – Carlo photons generated in the barrel region.

Figure 4 on page 5, Figure 5 on page 6, and Figure 6 on page 7 show for several photon energies the distribution of the variables F_4 and F_{Stki} (i = 1,3), fraction of energy in the 4 central towers of the cluster and in the 3 stacks, respectively.[1] For photons, all the energy is concentrated in 4 towers. In any case F_{Stk3} is below 0.4, and F_4 above 0.75. The peak at 0 in the distribution of F_{Stk1} is due to the threshold applied in the clustering or to photons not interacting in stack 1.

- *HIGH ENERGY PHOTONS*

At high energy, the two photons from a π^0 decay are too close to be resolved by the apparatus and it is in general impossible to distinguish a π^0 from a photon. The efficiency and the rejection power of several possible variables and cuts have been studied. The longitudinal profile of showers generated by

[1] Here F_4 is defined by $\frac{E_4}{E_{Corrected}}$ (where E_4 is computed from PEST, and $E_{Corrected}$ is taken from the PECO Bank)

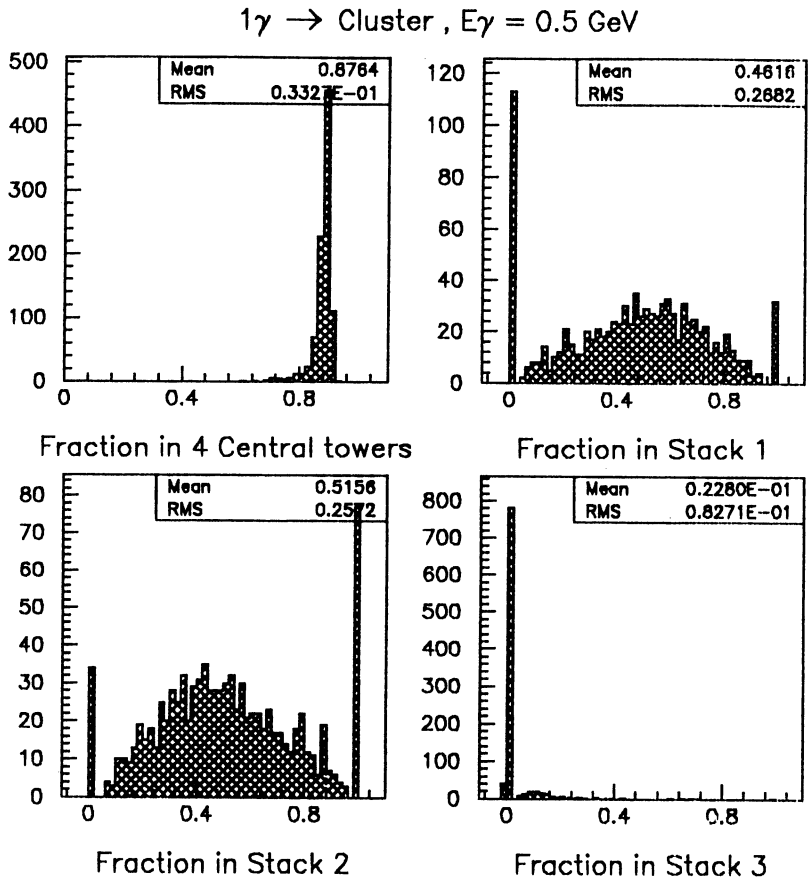

Figure 4: Lateral and longitudinal profile variables for single photons of 0.5 GeV. Determined on single Monte−Carlo γ's, generated in the barre region. Definitions of variables are given in the text.

a single photon or two photons from a π^0 decay are not significantly different. Variables based on the transverse profile have been studied instead.

Figure 7 on page 8 shows the distribution of the variable F_4 for π^0's and photons of different energies. Up to 15 GeV it is possible to discriminate π^0's from photons.

Another way to look at the lateral energy distribution in a cluster is to compute the axes of an ellipse defined in the θ,ϕ plane by the moments of the energy deposition around the cluster centroid. Figure 8 on page 9 shows the distribution of the ellipse big axis for various photon and π^0 energies. π^0's are not better separated from photons than previously (similar distributions are produced with any combination of the big and the small axis of the ellipse).

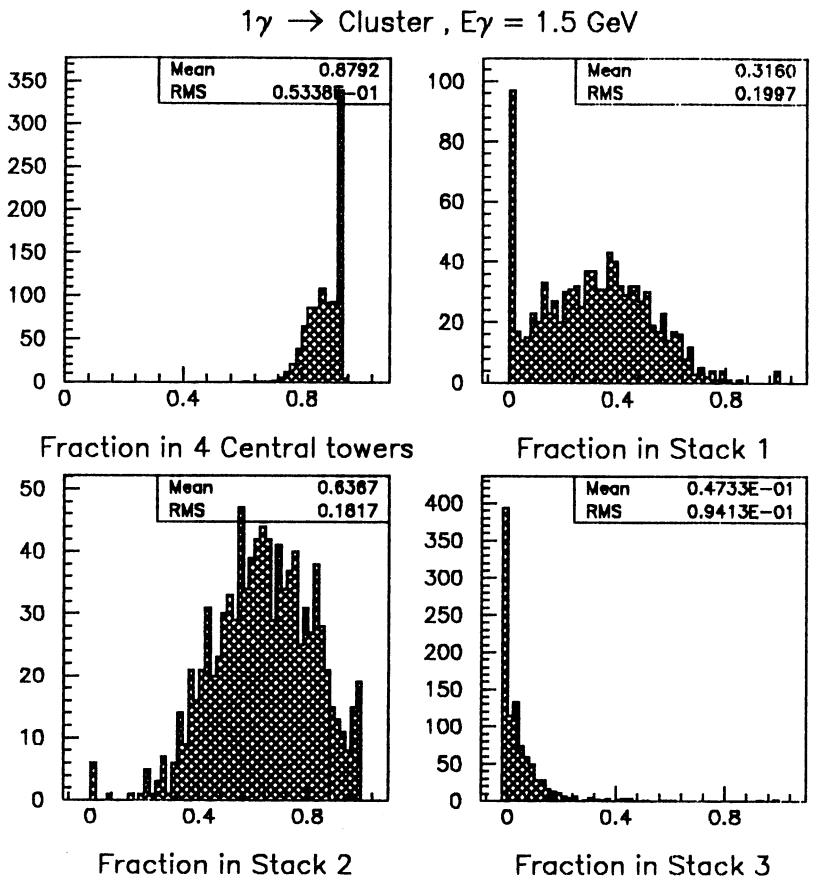

Figure 5: Lateral and longitudinal profile variables for single photons of 1.5 GeV. Determined on single Monte−Carlo γ's, generated in the barre region. Definitions of variables are given in the text.

To be more quantitative, Figure 9 on page 10 shows for several variables and cut values, the evolution of single photon efficiency and of the fraction of π^0's classified as photons. Above 20 GeV, no significant difference is obtained by the different methods.

2.3 Photon spectrum

From the above study, simple criteria to define photons have been derived.

In the following, a photon is a cluster with :

1. no track associated
2. a small lateral extension : $F_4 \geq 0.75$

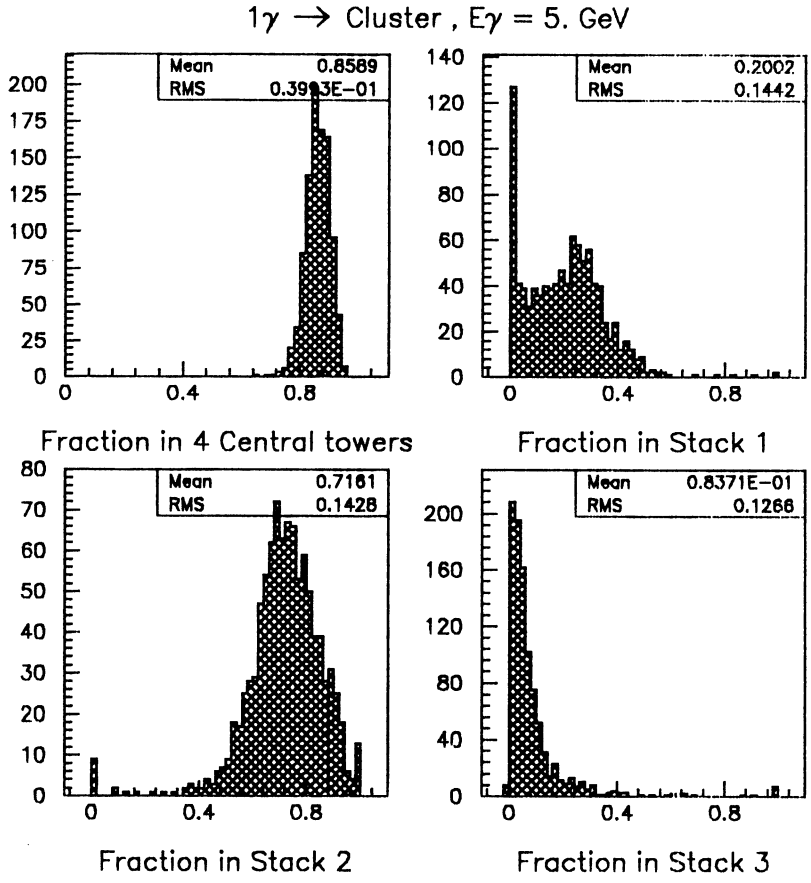

Figure 6: Lateral and longitudinal profile variables for single photons of 5. GeV. Determined on single Monte−Carlo γ's, generated in the barre region. Definitions of variables are given in the text.

3. an energy deposition concentrated in the first two stacks : $F_{Stk3} \leq 0.4$

Figure 10 on page 11 shows the efficiency of the above selection, as a function of energy, for single γ's which have generated a cluster in the ECAL. The efficiency is above 95 %, nearly independent of energy. The global photon efficiency is the product of this efficiency and the clustering efficiency (Figure 3 on page 4).

In addition we do not consider clusters which are in the overlap region ($\theta_{address} > 168$ or $\theta_{address} < 60$) and less than two towers apart from a crack between two adjacent modules in ϕ (this corresponds to a loss of 13% of the solid angle).

Figure 11 on page 12 shows the energy spectrum of the photon candidates.

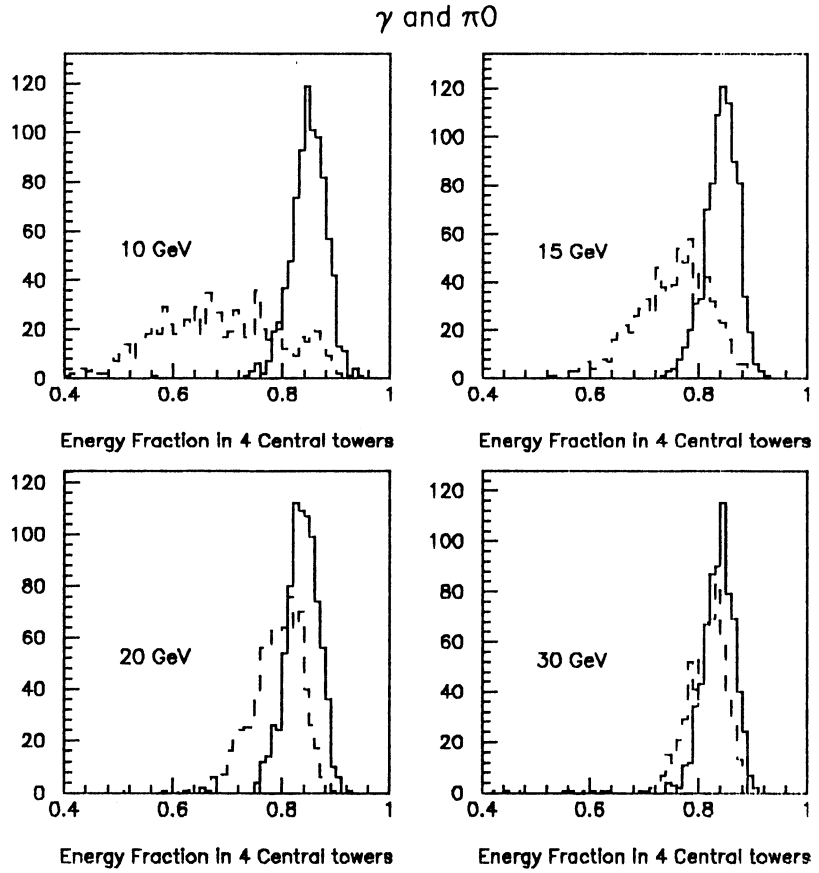

Figure 7: Lateral profile variable for single π^0's and photons. Determined on single Monte – Carlo particles, generated in the barrel region.

2.4 Comparison between DATA and Monte – Carlo hadronic events

2.4.1 The ECAL on real data and corrections to clusters

- *BAD CARDS EXIST EVEN AFTER CLEANING*

During JULIA processing a standard procedure is applied to ECAL data in order to remove 'pathological' storeys. However, as it can be seen on Figure 12 on page 13, some noisy electronic cards are still present. In this figure the θ,ϕ distribution of the leading neutral clusters above 5 GeV is shown. Accumulations due to noisy cards are clearly visible. These clusters have been removed from the analysis using a simple algorithm (see routine S4CLUS given in appendix). One noisy electronic card produces a typical pattern of 16 towers in ϕ times 2 towers in θ. An example of such a cluster is given on Figure 13 on page 14.

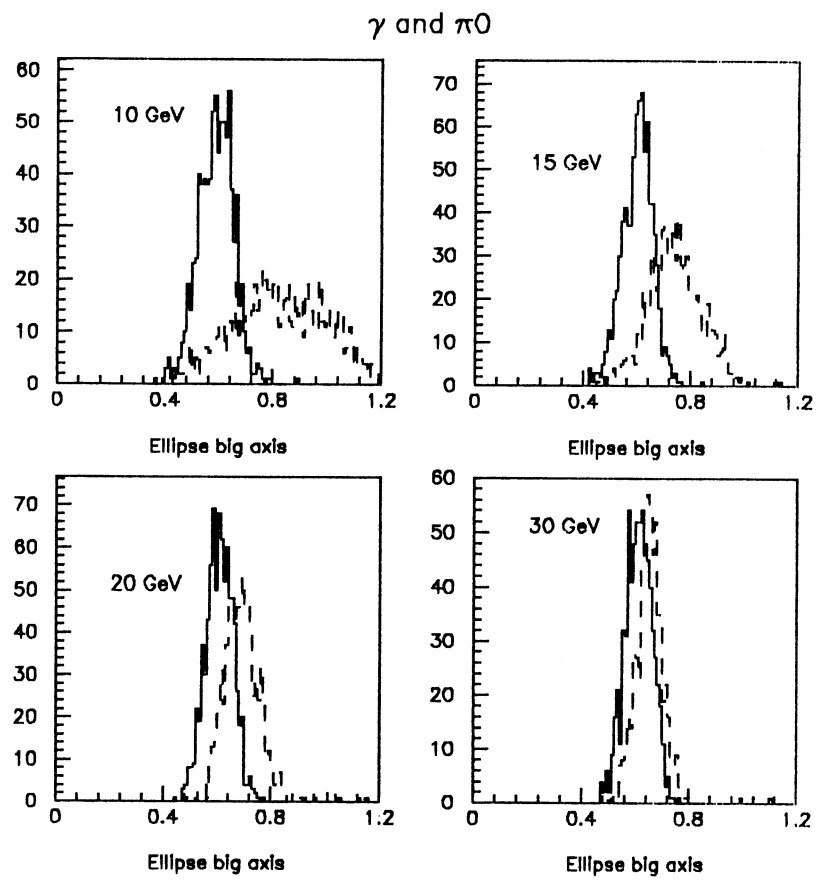

Figure 8: Ellipse big axis (in cell units) of lateral profile for single π^0's and photons. Determined on single Monte − Carlo particles, generated in the barrel region.

- *ENERGY CORRECTIONS*

Cluster energies are corrected inside JULIA, there are three principal corrections :

— *Clustering correction*
This correction is applied to all clusters and takes into account the energy losses due to the on line thresholds (20 , 28, 42 MeV for Stack 1, 2, 3 respectively in the Barrel) and the 30 MeV cut − off applied in the clustering procedure. In the barrel, the correction is given by the formula : $\Delta E = 0.125 - 0.0214 \times \sqrt{E_{raw}}$.

— *Corrections in cracks and overlap*
Energies of clusters in the overlap region [1] and in the vicinity of the boundary between two modules ('cracks') are corrected in the JULIA processing.
A correction of $\approx 1 GeV$ is applied to all clusters (regardless to their energy) which are near a crack (main tower at less than 2 pad rows from the boundary). This may not be appropriate.

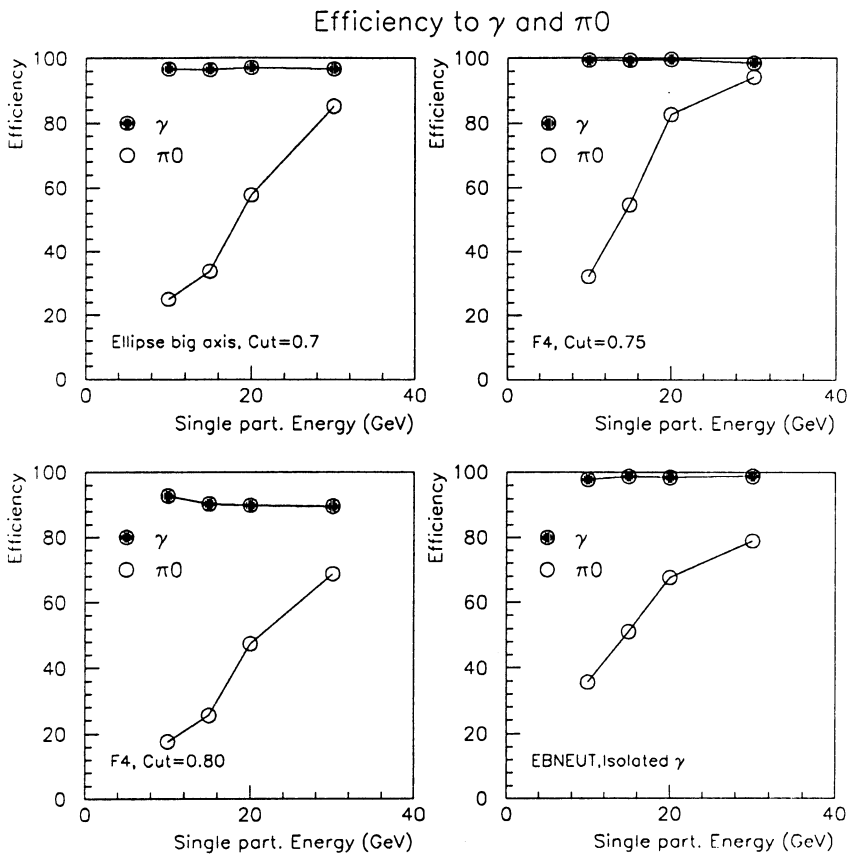

Figure 9: Efficiency to photons and π^0s misidentification at high energy. Determined on single Monte – Carlo particles, generated in the barrel region.

— *Correction from Bhabhas.*
Bhabha events are used to compute additional correction factors as described in [3].

2.4.2 Does the Monte – Carlo reproduce the data ?

Before comparing data to Monte – Carlo, a few points have to be noted :

1. Inside GALEPH thresholds on all storeys are set to 30 MeV but cluster energies are corrected inside JULIA for the online thresholds values.
2. There are neither 'Dead' nor 'Killed' storeys for Monte – Carlo data.

- *LONGITUDINAL AND TRANSVERSE VARIABLES*

Figure 15 on page 16 shows for neutral clusters (in the barrel) above 300 MeV, distributions of the variables F_4 , F_{Stki} (i = stack number). The same distribution is shown on Figure 16 on page 17 for Monte – Carlo events. These distributions are in good agreement, but one can notice small differences in the F_{Stki} distributions and a wider F_4 distribution in the data compared to the Monte – Carlo. Fig-

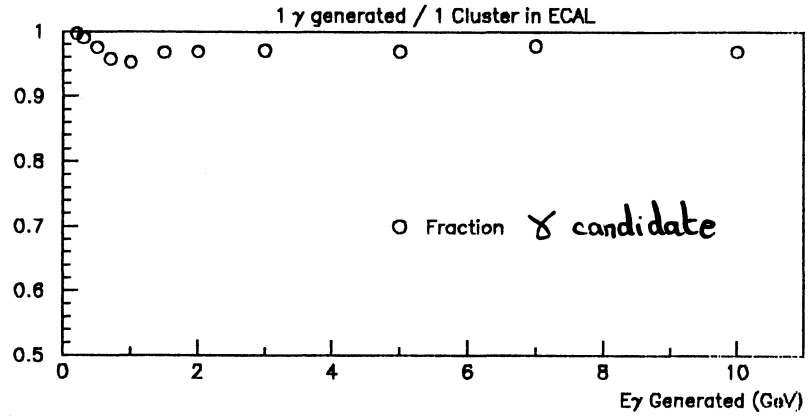

Figure 10: Efficiency of the photon criteria as a function of energy. Effiency determined on Monte−Carlo single photons in the barrel which result in one cluster.

ure 17 on page 18 shows the ratio of data to Monte−Carlo for these longitudinal and transverse variables, differences mentioned above are clearly visible. One potential source for this discrepancy is the tendency of the clustering to merge nearby clusters. An example is given on Figure 14 on page 15 which is showing a cluster made out of three clearly separated clusters. All the benefit of the high transverse granularity of the calorimeter is lost. It is unlikely that the MC reproduces such cluster merging correctly.

- *NUMBER OF CLUSTERS PER EVENT*

Figure 18 on page 19 shows the number of neutral clusters above 300 MeV observed in the barrel, before and after the photon criteria have been applied. The distribution is shown in Figure 19 on page 20 for Monte−Carlo data. Discrepancy between real and simulated data are clearly visible when the photon criteria is applied (1.2 more photon candidate per event in average in the Monte−Carlo). We have checked that this difference is independent of the energy cut applied. Furthermore, this discrepancy is of the same order (20% more clusters) for charged electromagnetic clusters fulfilling photon criteria.

- *NUMBER OF TOWERS PER CLUSTER*

It appears that the Monte−Carlo tends to produce more electromagnetic clusters than the data. There is also a small difference in the cluster size, as it can be seen in Figure 20 on page 21 showing the number of towers per cluster.

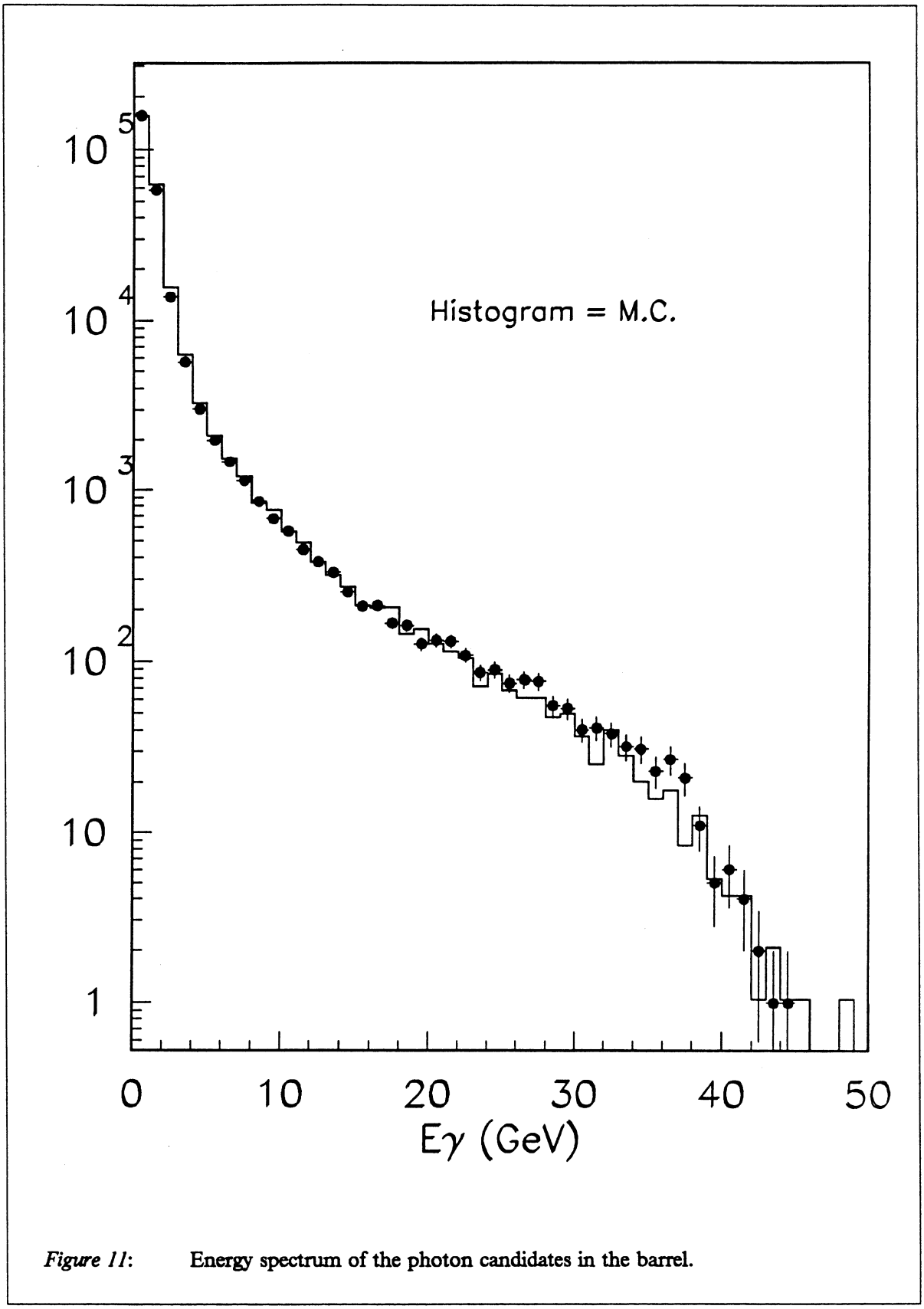

Figure 11: Energy spectrum of the photon candidates in the barrel.

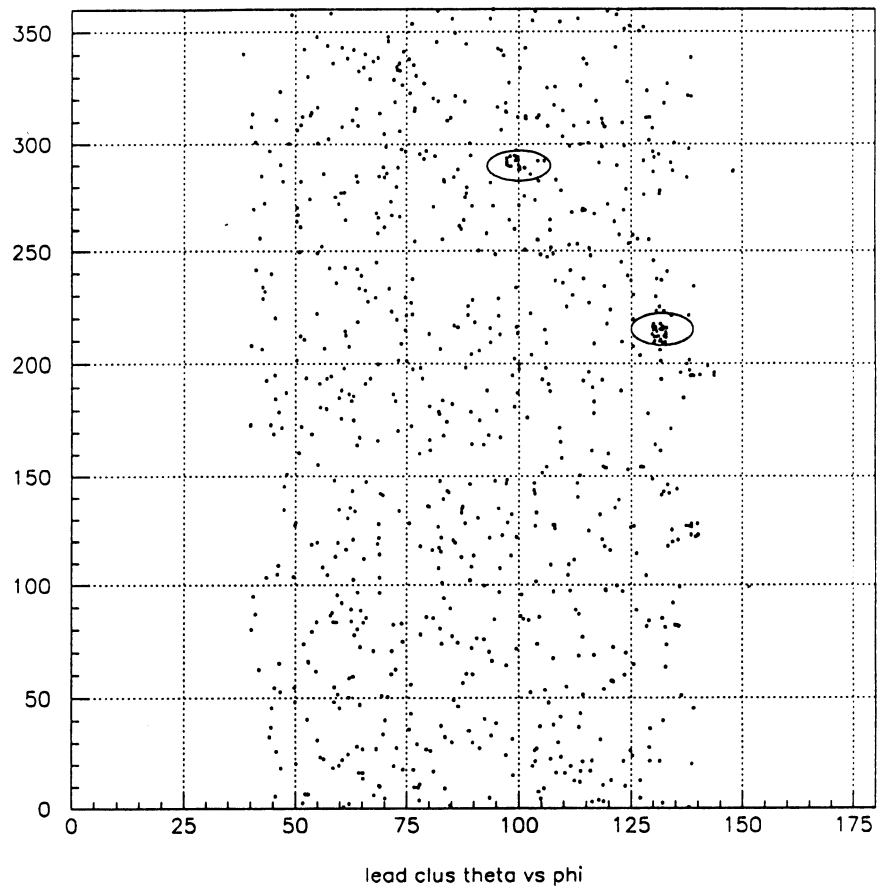

Figure 12: Theta , phi distribution of neutral clusters above 5 GeV in the Barrel. Accumulations due to 'bad' electronic cards are clearly visible.

- *EFFECT OF 'DEAD' AND 'KILLED' STOREYS*

We have investigated if the differences between simulated and real data, on the distributions of F_{Stki} and F_4 (which may explain the difference in terms of number of neutral photon candidate clusters per event) can be due to :

- Dead/killed storeys not implemented in the Monte – Carlo simulation
- Differences on the energy thresholds (30 MeV on all stacks for Monte – Carlo, 20, 28 and 42 MeV on real data)

A sample of 1,000 events have been reprocessed through JULIA with the following modifications:

- the map of dead storeys (corresponding to runs ≥ 4800) has been put in the JULIA data cards (EDDB bank, 365 dead storeys)
- a mean map of killed storeys has also been put in the data cards (EKLS bank, this map is an average of killed storeys over all the hadronic events passing the selection given in 1.1 on page 1, 548 storeys)

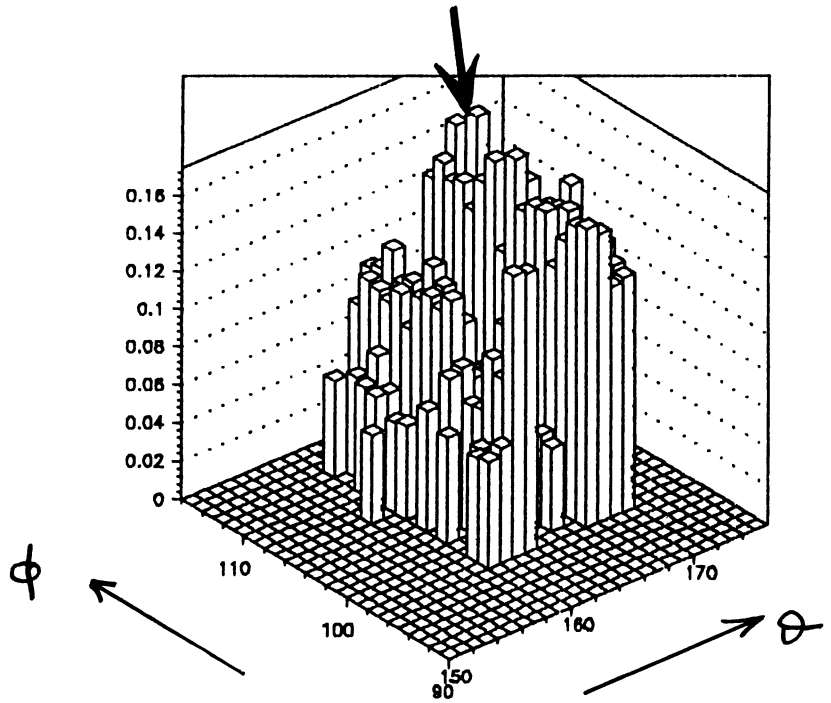

Figure 13: Tower energy profile of a cluster due to a bad electronic card. The vertical scale is in GeV. The horizontal scale refers to the tower number. Recall that in the barrel towers are numbered from 51 to 178 in θ and from 1 to 384 in ϕ. The displayed cluster is the PECO cluster number 13 in event 5049/3367. Its corrected energy is 8.8 GeV. All the energy is in stack 3.

— all storeys above 30 MeV but below online thresholds have been killed inside JULIA before event processing ($\approx$ 10.5 storeys/event)

No significant differences in the number of clusters per event (electromagnetic or not) are observed in the barrel after this reprocessing. In the End cap regions, however, a small difference is observed ($+0.3$ cluster per event, -0.2 electromagnetic cluster per event).

The excess of electromagnetic clusters in Monte−Carlo data, cannot be explained by detector effects (dead/killed storeys, thresholds) not included in the Monte−Carlo but rather by a lack of the Monte−Carlo simulation to reproduce the fluctuations and the shape of electromagnetic showers in the ECAL.

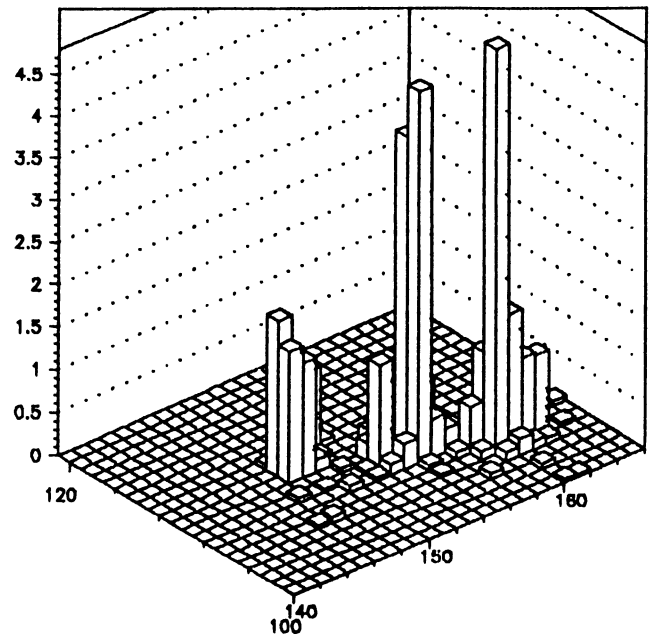

Figure 14: Tower energy profile of a cluster made out of 3 clusters. The displayed cluster is the PECO cluster number 9 in event 4981/2397. Its corrected energy is 31 GeV.

2.5 Conclusion

In this paragraph we have introduced very simple criteria to define photons in the ECAL. These criteria have an excellent efficiency on single photons and have been applied on clusters in hadronic events. However we have found some discrepancies between real and simulated data. It is not known wether the problem is due to the Monte − Carlo shower simulation or the inadequacy of the clustering algorithm for photons, or both.

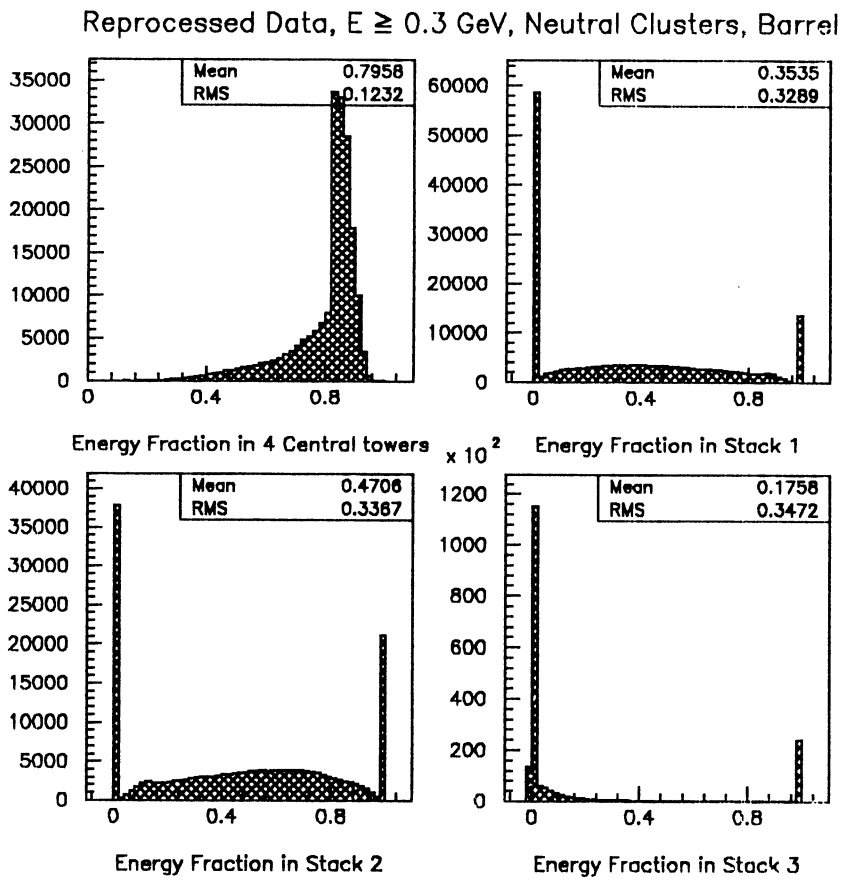

Figure 15: Data: Transverse and longitudinal variables distribution. All neutral clusters in barrel above 300 MeV.

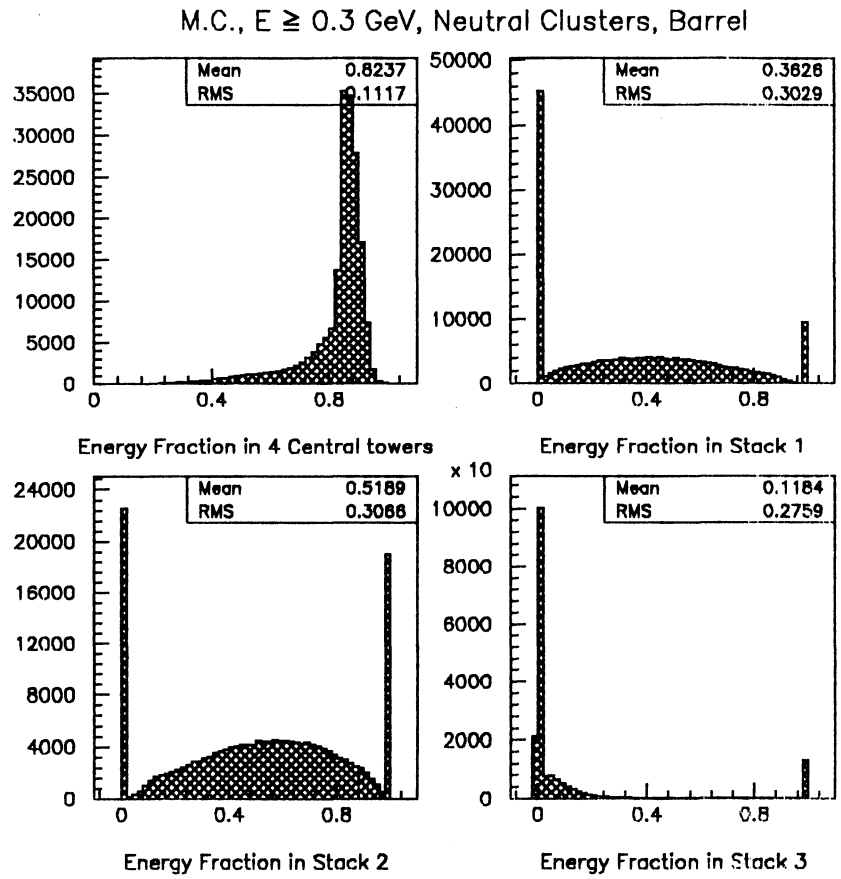

Figure 16: Monte – Carlo :Transverse and longitudinal variables distribution. All neutral clusters in barrel above 300 MeV.

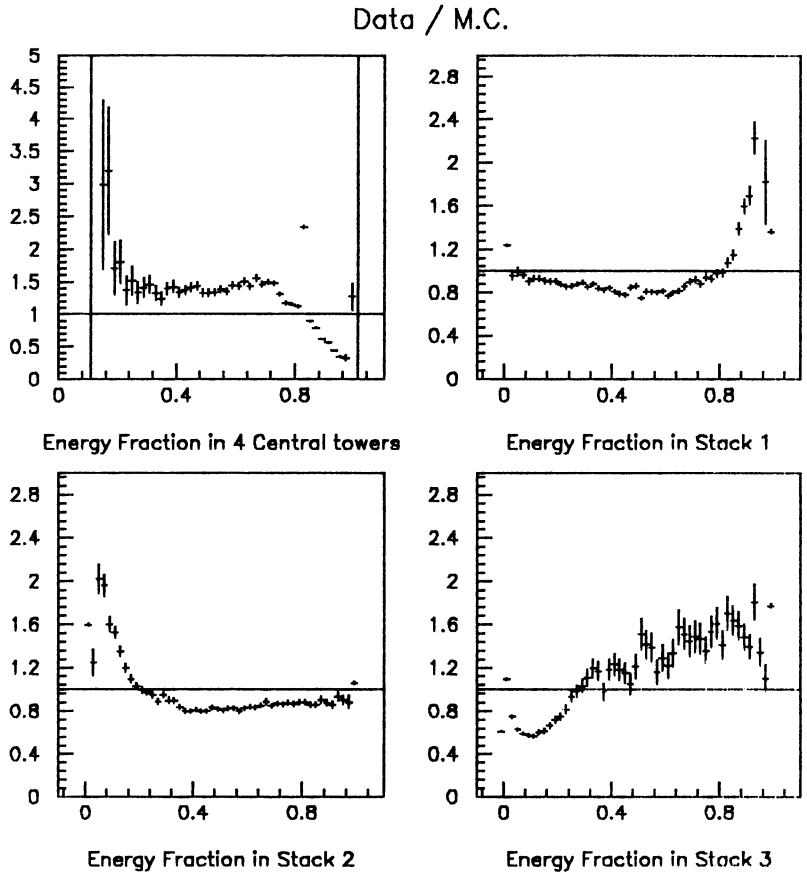

Figure 17: Data/Monte−Carlo: Transverse and longitudinal variables distribution. All neutral clusters in barrel above 300 MeV.

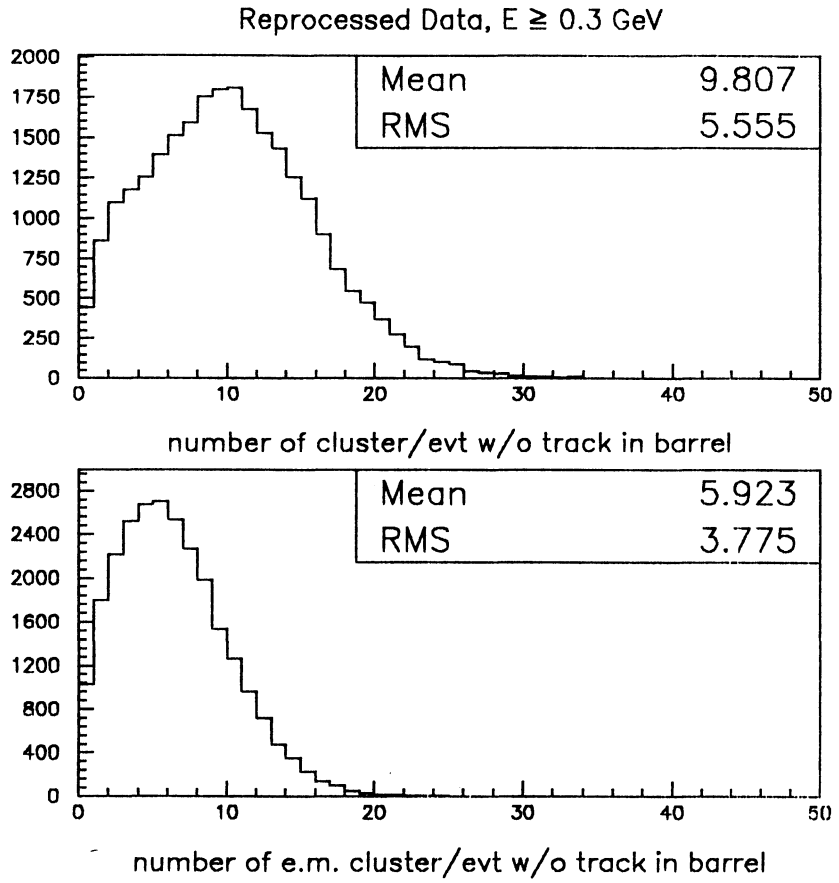

Figure 18: Data: Number of neutral clusters. Above 300 MeV in the Barrel, before and after photon selection.

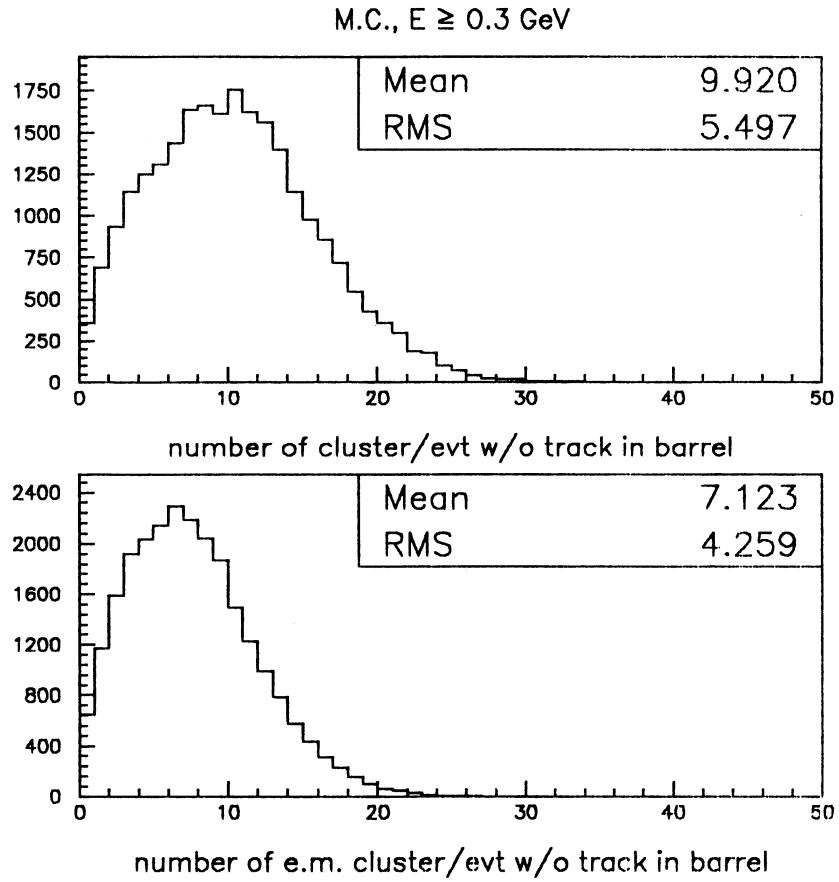

Figure 19: Monte−Carlo: Number of neutral clusters. Above 300 MeV in the Barrel, before and after photon selection.

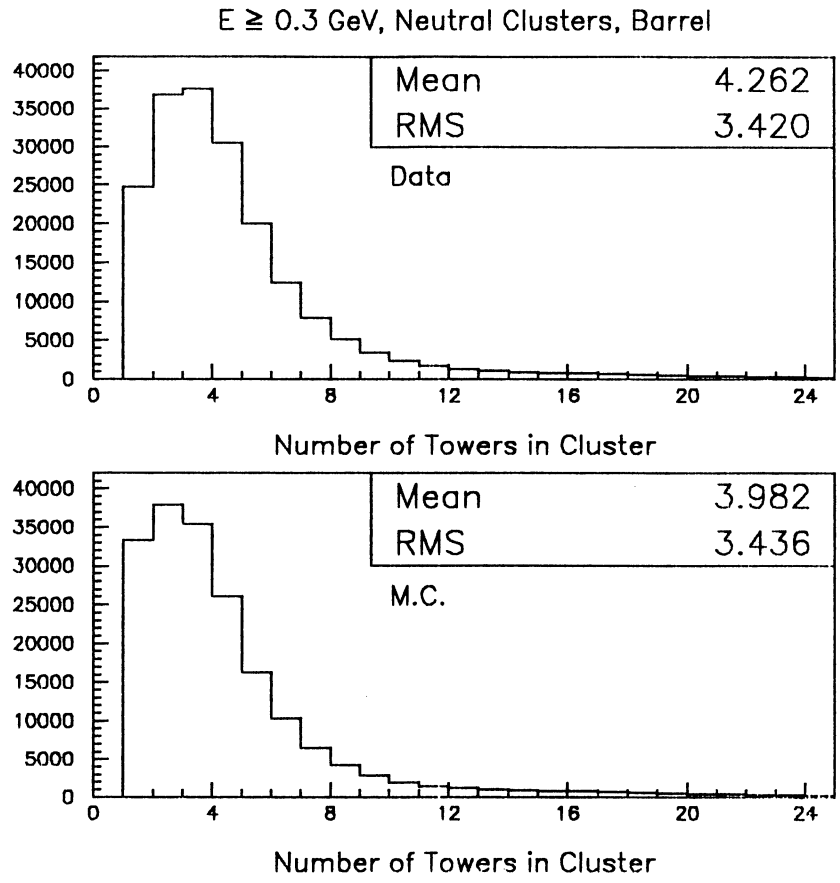

Figure 20: Cluster size. Number of towers per neutral electromagnetic cluster above 300 MeV, in the barrel, Data and Monte – Carlo

3. Inclusive production of π^0 in hadronic events.

The purpose here is to study the ECAL response to low energy photons and to measure the inclusive production of π^0's in hadronic events. One should keep in mind that the ECAL calibration has never been studied in the energy range covered in the analysis presented below. The low energy calibration of the calorimeter comes from $e^+e^- \rightarrow e^+e^-e^+e^-$ reactions with electron energies down to 2 GeV [3].

3.1 Introduction

In order to reconstruct π^0's from the invariant mass distribution of two photon candidates, one needs a good efficiency to detect low energy photons and a good energy resolution for those low energy photons.

- *NUMBER OF CLUSTERS FOR ONE SINGLE π^0*

Figure 21 on page 23 shows the percentage of π^0's resulting in one or two clusters in the barrel as a function of the initial particle energy generated with GALEPH. π^0's do not generally result in two clusters in the ECAL. At low energy one of the two decay photons may not be reconstructed, and at high energy the two photons collapse in one cluster. In the interval from 1 to 6 GeV, π^0's result in two clusters in more than 50 % of the cases. One can directly see from this figure that

- above 6 GeV it is impossible to get a good efficiency to reconstruct π^0's from the invariant mass of two photons
- already at maximum efficiency (between 2 and 3 GeV), 20% of π^0 do not give two clusters in the ECAL.

3.2 Observation of π^0 in Hadronic events

Only hadronic events as defined in 1.1 on page 1 have been used in the analysis presented below.

- *TWO PHOTON MASS DISTRIBUTION*

Figure 22 on page 24 shows the invariant mass distribution of any two photons above 300 MeV in the barrel for different cuts in π^0 momentum (E_π). To reduce the combinatorial background, the two photons have to be in the same hemisphere ($\cos\vec{\gamma}_1.\vec{\gamma}_2 > 0$). A clear π^0 signal is visible. This signal is more and more visible when the π^0 energy increases. For $E_\pi \leq$ 1 GeV, due to a poor energy resolution, no π^0 signal can be observed.

- *NUMBER OF π^0'S*

The number of π^0's is determined by a fit to the mass distribution assuming a gaussian shape for the signal and a polynomial for the background. Figure 23 on page 25 shows an example of such a fit for π^0 momentum above 2 GeV.

Above $E_\pi \geq 1$ one observes a total of 11179 π^0's. Table 1 on page 26 gives the evolution of the number of π^0 and the ratio signal over background, as a function of the π^0 energy (Signal is defined as the gaussian integral, background is defined as the integral of the polynomial in the interval $[M+3\sigma\ ,\ M-3\sigma]$. Background drastically decreases with E_π. The fact that the π^0 is found at the right mass value is a remarkable result.

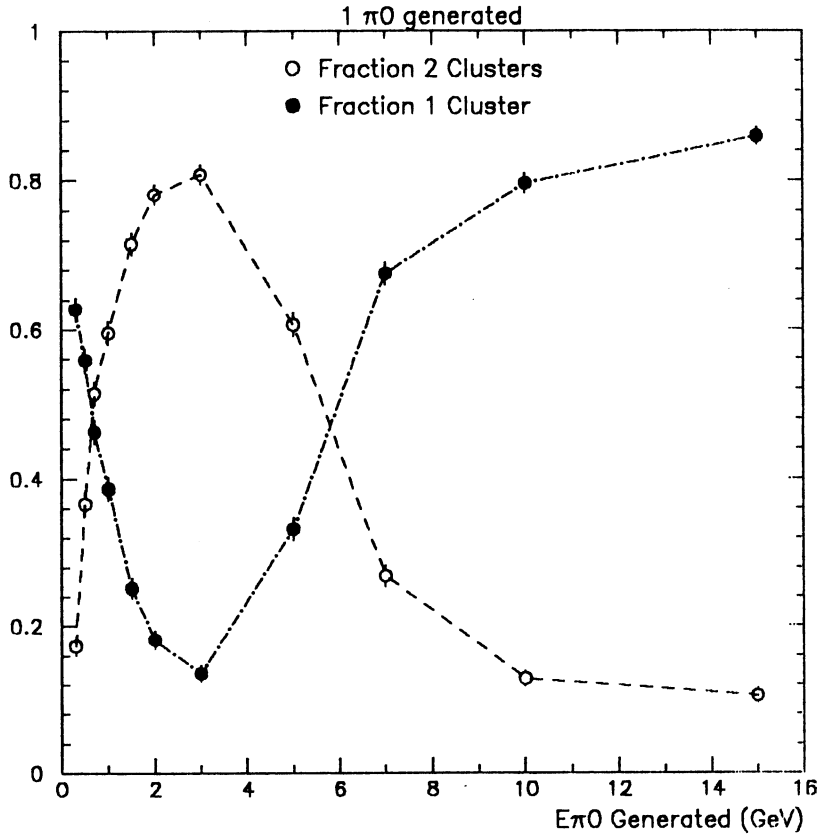

Figure 21: Fraction of π^0's resulting in one or zero clusters. Determined on single Monte – Carlo π^0 generated in the barrel region.

- *π^0 ENERGY SPECTRUM*

Figure 24 on page 27 shows the π^0 energy spectrum, from 1 to 7 GeV. Over this energy range the yield decreases by 2 orders of magnitude. Above 7 GeV there is not enough statistics left to observe a π^0 signal in the two photons mass distribution.

3.3 π^0's in Monte – Carlo events

- *MASS DISTRIBUTION*

Figure 25 on page 28, shows the two photon mass distribution obtained from Monte – Carlo, for various E_π conditions. Figure 26 on page 29 compares the mass distribution obtained from data and Monte – Carlo for $E_\pi \geq 2$ GeV.

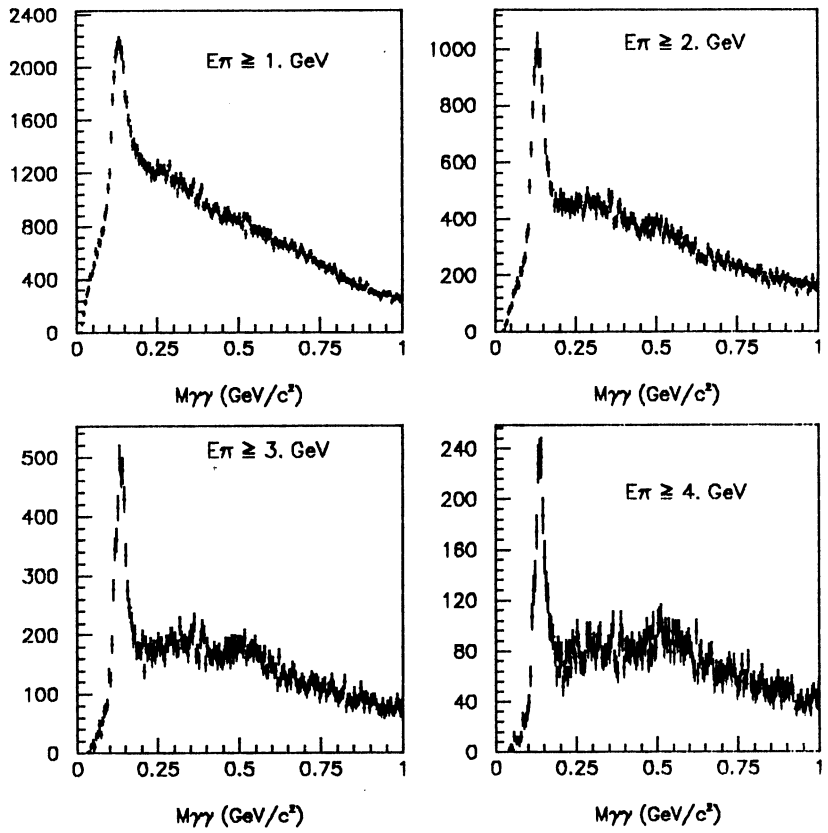

Figure 22: Data : Two photon mass distribution. Barrel region, $E_\gamma \geq 300\ MeV$

The ratio signal over background is given in Table 2 on page 30 as a function of E_π (normalized to the same number of hadronic events), one can already notice an excess of π^0's in the Monte−Carlo, signal over background being of the same order and a systematic shift of the π^0 mass ($\approx$ 5 MeV).

- *π° ENERGY SPECTRUM*

Figure 27 on page 30, shows the ratio of the π^0 energy spectrum determined in real data over Monte−Carlo data (normalized to the same number of hadronic events), in average 18% more π^0 are reconstructed from Monte−Carlo. This excess could be related to the 20% excess of photon candidates observed in Monte−Carlo data 2.4.2 on page 10.

- *π^0 ACCEPTANCE*

Figure 28 on page 31, shows the ratio of the number of reconstructed π^0 over the number of generated ones in the barrel, as a function of energy. At maximum, π^0 are reconstructed with an efficiency of 20% (at 3 GeV). This efficiency is rather constant but drops below 10 % above 5 GeV when photons from π^0 decay begin to merge into one cluster. Such a poor efficiency cannot be explained by the fiducial cuts applied ('cracks' and 'overlap' regions rejected) nor by the energy cut on the photons, a large fraction of π^0s are lost in hadronic events. The efficiency to reconstruct single photons is high, but in

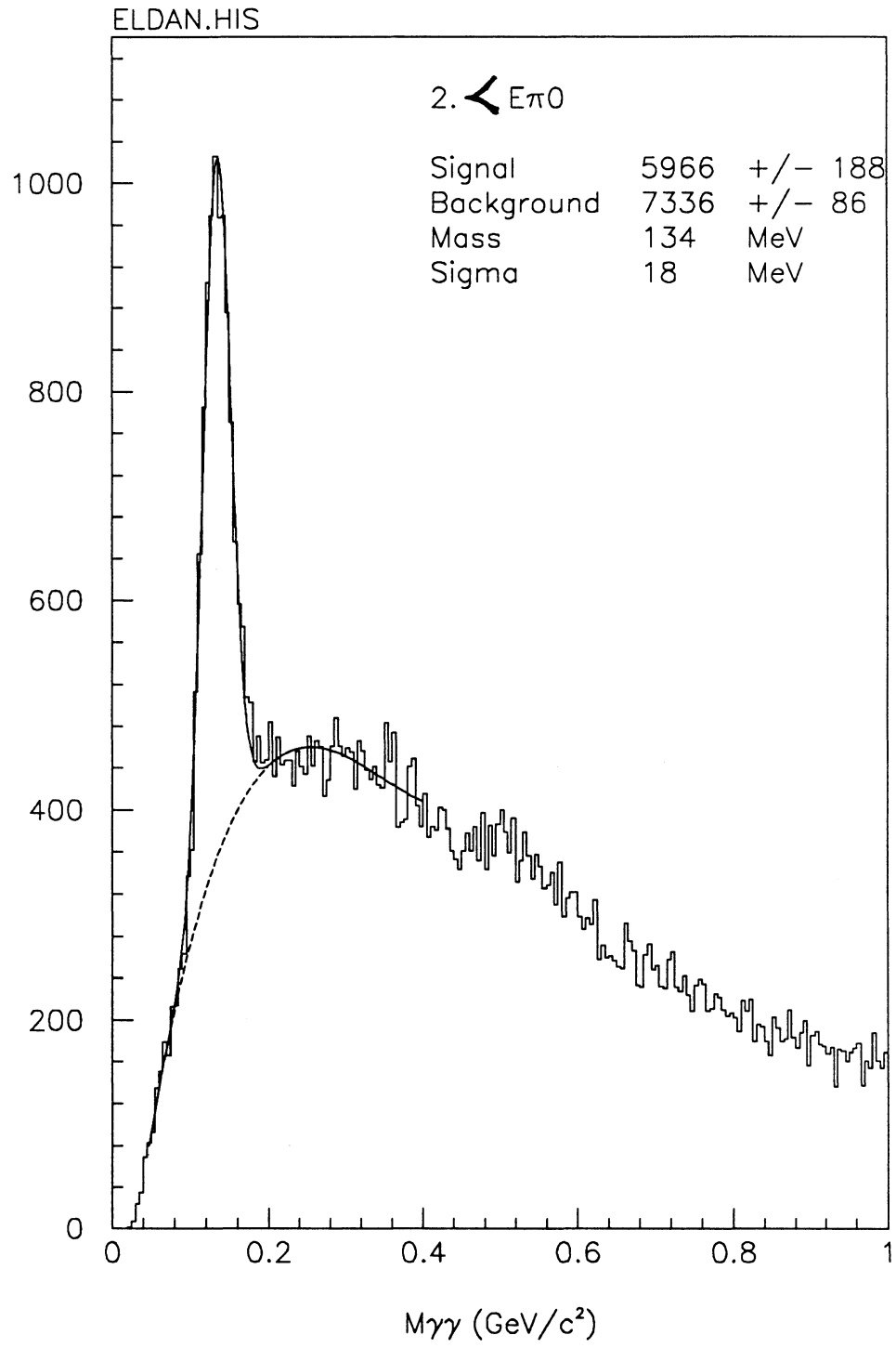

Figure 23: **Example of a fit to the two photon mass distribution.**

Table 1: Number of π^0 on Real Data for various π^0 momentum ranges

Determined in the barrel region, each photon above 300 MeV. MC is normalised to the number of data events.

E range (GeV)	Signal	Signal/Backgound	Mass , sigma (MeV)
≥ 1	11179	0.44	133 , 20
≥ 2	5966	0.81	134 , 18
≥ 3	3180	1.31	135 , 18
≥ 4	1540	1.78	138 , 17
1 − 2	5241	0.27	132 , 23
2 − 3	2798	0.57	133 , 18
3 − 4	1706	1.14	133 , 18
4 − 5	926	2.04	137 , 17
5 − 6	382	1.85	140 , 18
6 − 7	129	1.50	143 , 18

hadronic events due to the clustering properties photons are often merged in clusters of several particles.

3.4 Systematics

In order to study the systematics in the determination of the number of π^0 per event, several checks have been performed.

1. *ASYMMETRY CUT*

One expects the energy asymmetry between two photons from a π^0 decay to have a flat distribution between 0 and 1. This is not the case for wrong combinations where the distribution is strongly peaked around 1. (the asymmetry is defined by $A = \frac{E_1 - E_2}{E_1 + E_2 - 2E_{\gamma min}}$ where $E_{\gamma min}$ is the minimum photon energy considered., $E_{\gamma min}$ = 300 MeV in our case, E_1 and E_2 being the two photon energies).

Figure 29 on page 32, shows the asymmetry distribution for all combinations of photons and for photons having an invariant mass between 100 and 200 MeV. In both cases the distribution is not flat.

One increases the ratio signal over background by requiring the asymmetry to be small. Figure 30 on page 33 shows the evolution of the number of π^0 and background as a function of the asymmetry cut, evolution of signal over background is also shown on the figure. As expected this ratio increases when asymmetry decreases, but not by more than 20 %.

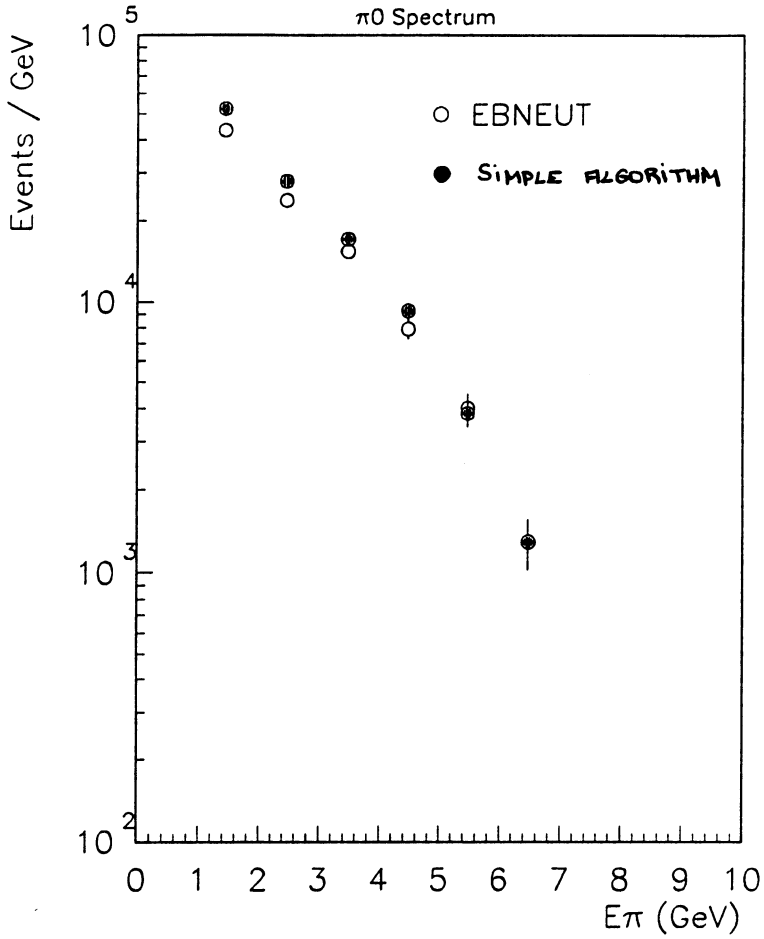

Figure 24: Data: π^0 energy spectrum in the barrel.

If the method to determine the number of π^0 from the mass distribution is correct, one has the following relation : $\frac{N_1}{A_1} = \frac{N_2}{A_2}$ where N_i is the number of π^0 determined with the cut A_i on the asymmetry. Figure 31 on page 34, shows the evolution of $\frac{N_i}{N_0 A_i}$ as a function of the asymmetry cut A_i (N_0 being the number of π^0 when no asymmetry cut is applied). Within 2.5%, the results are consistent. A value around 0.8 for the asymmetry cut seems optimal.

2. *MINIMUM ENERGY*

Figure 32 on page 35 shows the evolution of the two photon mass for different minimum photon energy ($E_\gamma \geq$ 1 GeV). Background decreases when $E\gamma$min increases (Table 3 on page 35), the π^0 Mass and the sigma being unchanged. $E\gamma$min was set to 300 MeV in order to get a good π^0 efficiency. If one requires a better signal over background ratio keeping a reasonable efficiency, $E\gamma$min of 500 MeV can

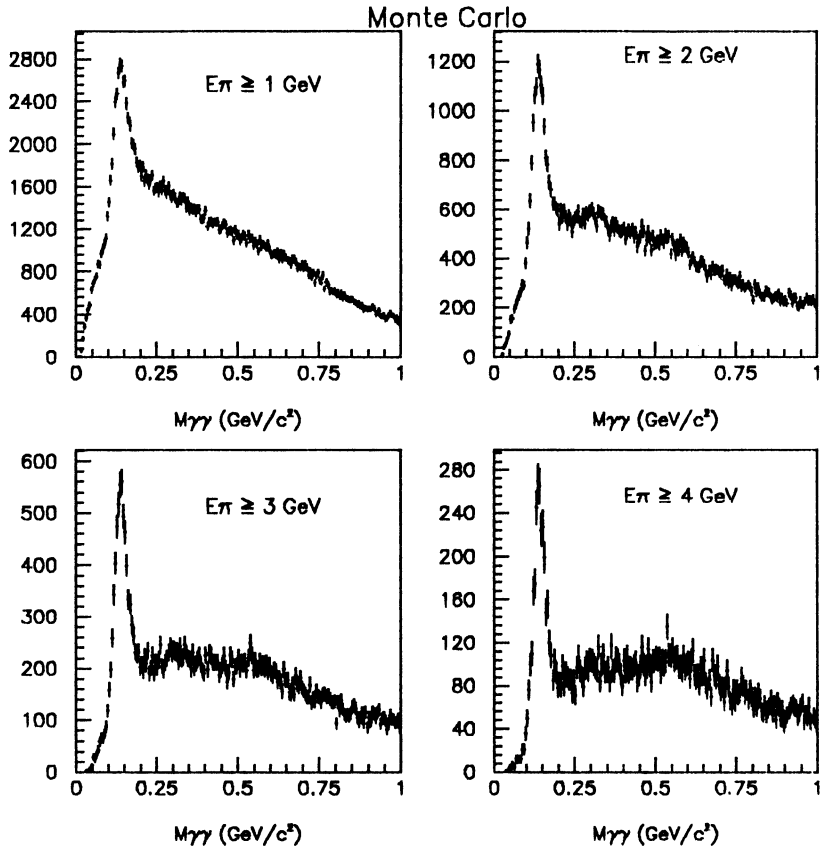

Figure 25: Monte−Carlo: Two photon mass distribution. Barrel region, $E_\gamma \geq 300\ MeV$

be an alternative.

3. *FITTING PROCEDURE*

We have checked that the number of π^0's as well as the signal over background and π^0 mass remain unchanged (within errors) when the fitting interval or the polynomial form are changed.

4. *EBNEUT PACKAGE*

A more sophisticated way to define photons is to use the EBNEUT [2] package. For a given cluster in the ECAL, this package proceeds in two steps:

a. it first determines, from the longitudinal profile in the three stacks, if the cluster is electromagnetic (IFOT(16)); the cluster can be *electromagnetic* , *hadronic* or

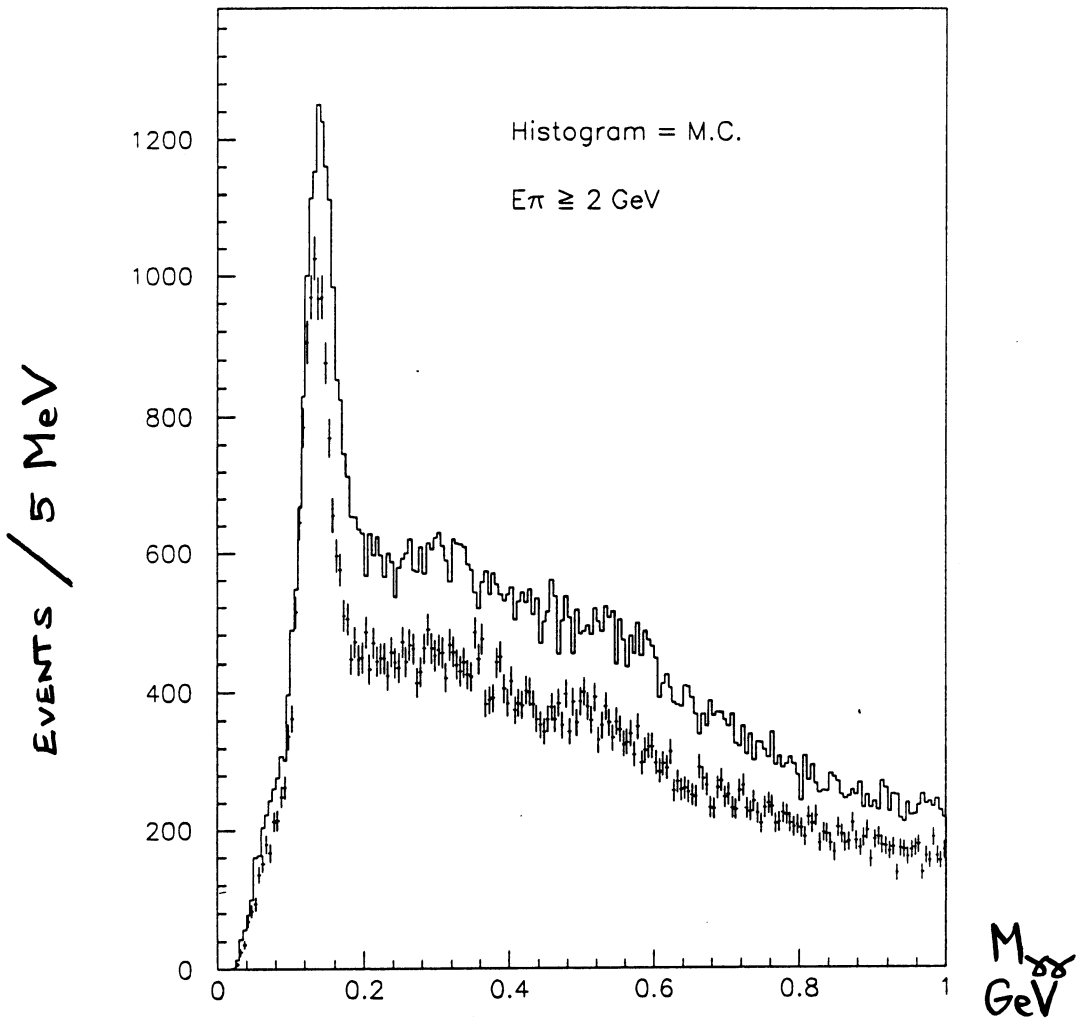

Figure 26: Two photon mass distribution data and Monte−Carlo. Barrel region, $E_\gamma \geq 300\ MeV$ and $E_\pi \geq 2$ GeV.

ambiguous.

b. from the transverse profile, the cluster is then classified as (IFOT(18)) *single isolated photon, unresolved multi−gammas, purely hadronic, etc...*,clusters classified as *ambiguous* at the first step can be called *isolated photon* at the second step.

Performance of this package was first evaluated on single photons generated in the barrel region. Figure 33 on page 36 shows as a function of energy the cluster classification given by EBNEUT. From that figure, one can notice :

- below 2 GeV ≈ 20 % of the photons are classified as *hadronic* clusters.
- above 2 GeV, ≈ 10 % of the photons are classified as *ambiguous* but all of them are then called isolated photon.
- below 1.5 GeV, efficiency of this package is less than 80 %

Table 2: Number of π^0 on M.C. for various π^0 momentum ranges

Determined in the barrel region, each photon above 300 MeV.

E range (GeV)	Signal	Signal/Backgound	Mass , sigma (MeV)
≥ 1	13165	0.37	140 , 22
≥ 2	6747	0.70	140 , 19
≥ 3	3738	1.24	140 , 19
≥ 4	1905	1.95	142 , 19
1 – 2	6668	0.24	142 , 26
2 – 3	3084	0.46	140 , 20
3 – 4	1857	0.95	137 , 19
4 – 5	1160	2.14	142 , 19
5 – 6	468	2.15	143 , 20
6 – 7	124	1.24	144 , 15

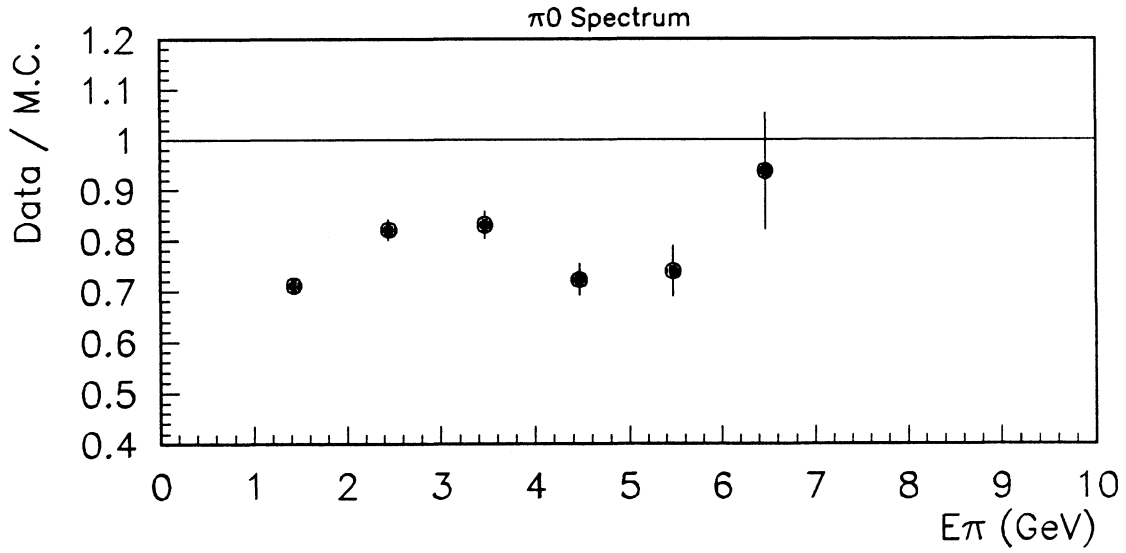

Figure 27: π^0 energy spectrum. Ratio Data over Monte – Carlo

Figure 34 on page 37 compares the efficiency, on single photons, of EBNEUT and photon criteria defined in this note. At high energy (above 4 GeV) the two methods are equivalent, at low energy the EBNEUT efficiency drops drastically while the simple photon criteria efficiency remains constant. As a consequence, EBNEUT will be less efficient on π^0.

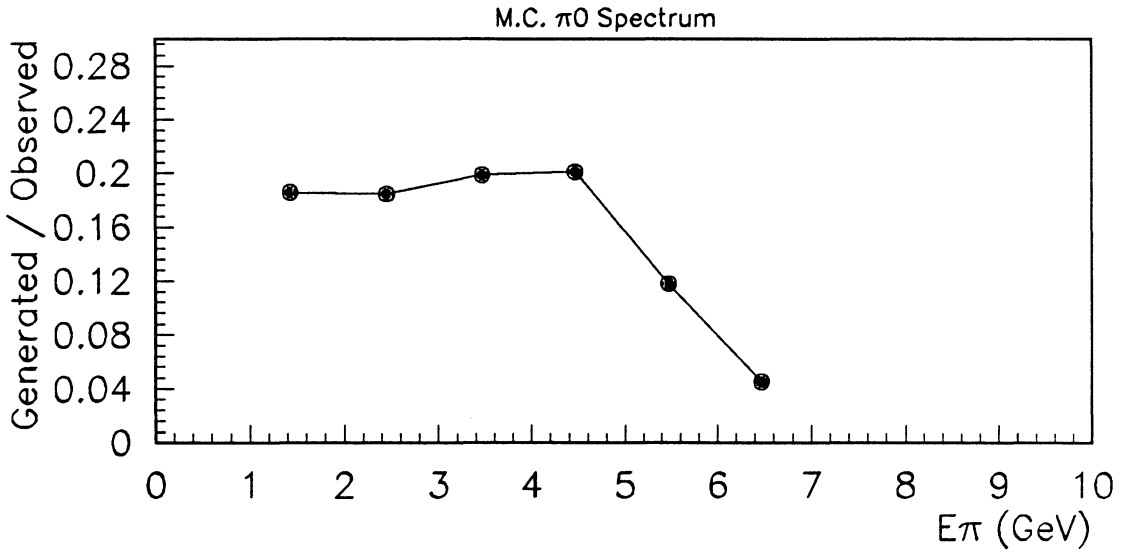

Figure 28: Efficiency to reconstruct π^0. Determined on Monte−Carlo hadronic events, from the two photon mass distribution in the barrel.

Figure 35 on page 38 shows the two photon mass distribution obtained using EBNEUT (Barrel region, cracks and overlap removed , IER = 0) for different $E\gamma$min values. Details are given in Table 4 on page 38. Compared to the simple algorithm (Table 2 on page 30), for $E_\gamma \geq 1$ GeV, one gets 15% less π^0 with 34% less background. This comparison is biased : by construction, EBNEUT is less efficient for low energy π^0's where the background is higher.

3.5 Search for η meson

Search of η meson decays into two photons, requires a very good energy resolution. In addition one has to reject background coming from decays of π^0's. η's are searched from two photon mass combinations where none of the photons contribute with any other photon in the event to a π^0 mass with an asymmetry less than 0.8. Figure 36 on page 39 shows the mass distribution of such photon pairs for various minimum energy cuts. An η signal emerges from the combinatorial background above 1 GeV of minimum photon energy.

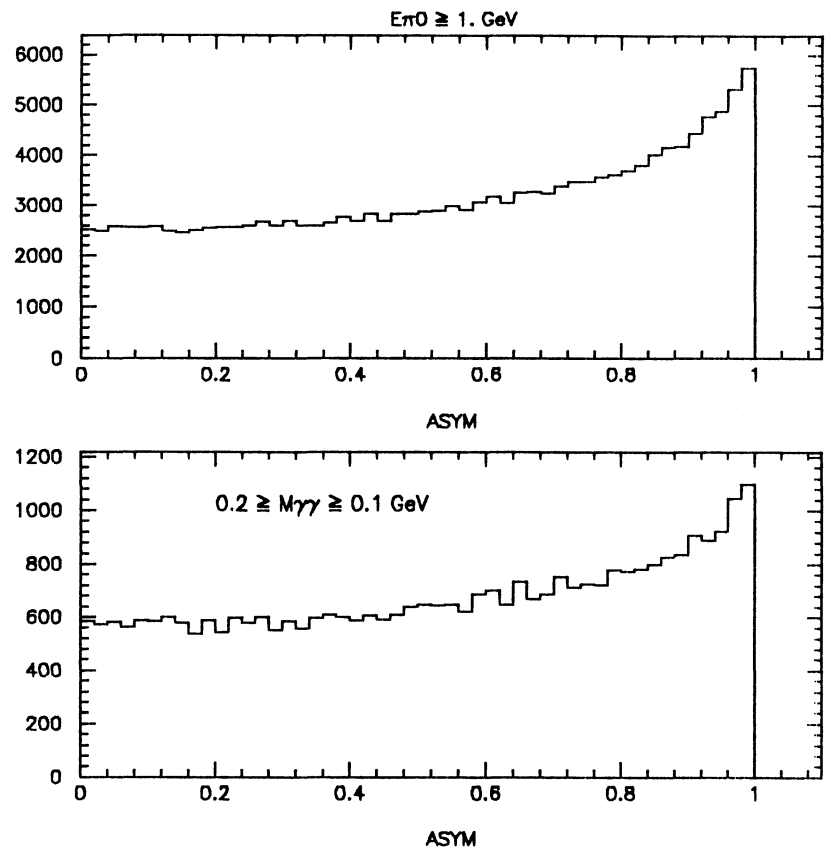

Figure 29: Asymmetry distribution for all photons. and those in the π^0 mass region.

3.6 Conclusion

Using a simple photon algorithm, a clear π^0 signal has been observed, at the right mass. The π^0 energy spectrum has been derived and an excess of π^0 has been found in the Monte−Carlo. It is not clear if this excess is real or due to a bad simulation of low energy electromagnetic showers in the ECAL. Systematics in the determination of the π^0 energy spectrum have been discussed in some details. A η signal has also been observed.

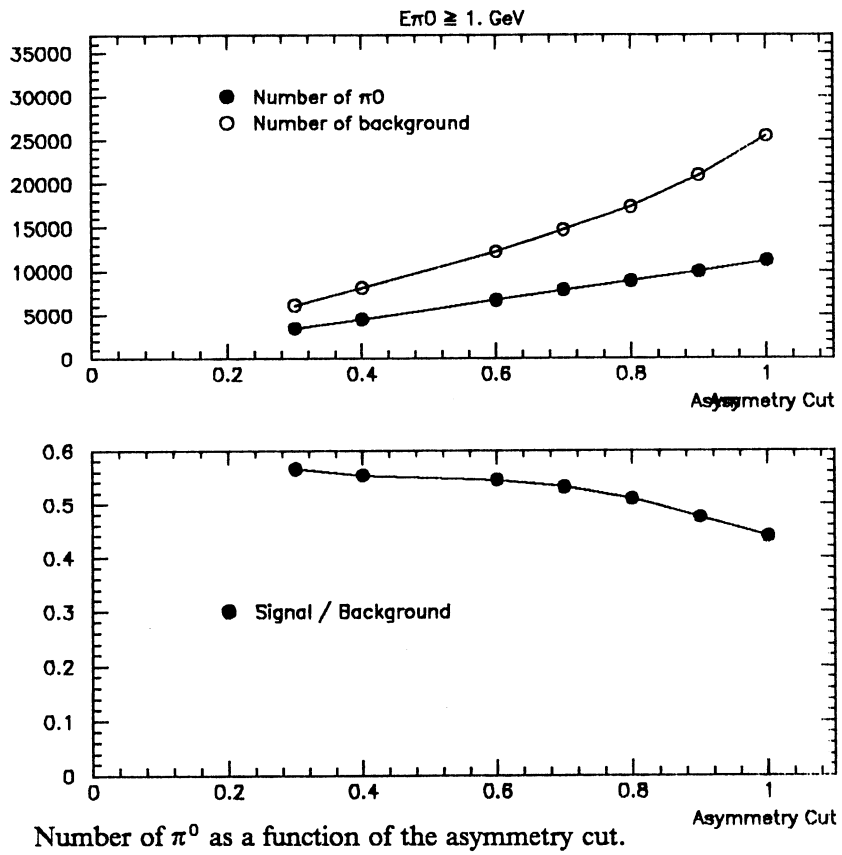

Figure 30: Number of π^0 as a function of the asymmetry cut.

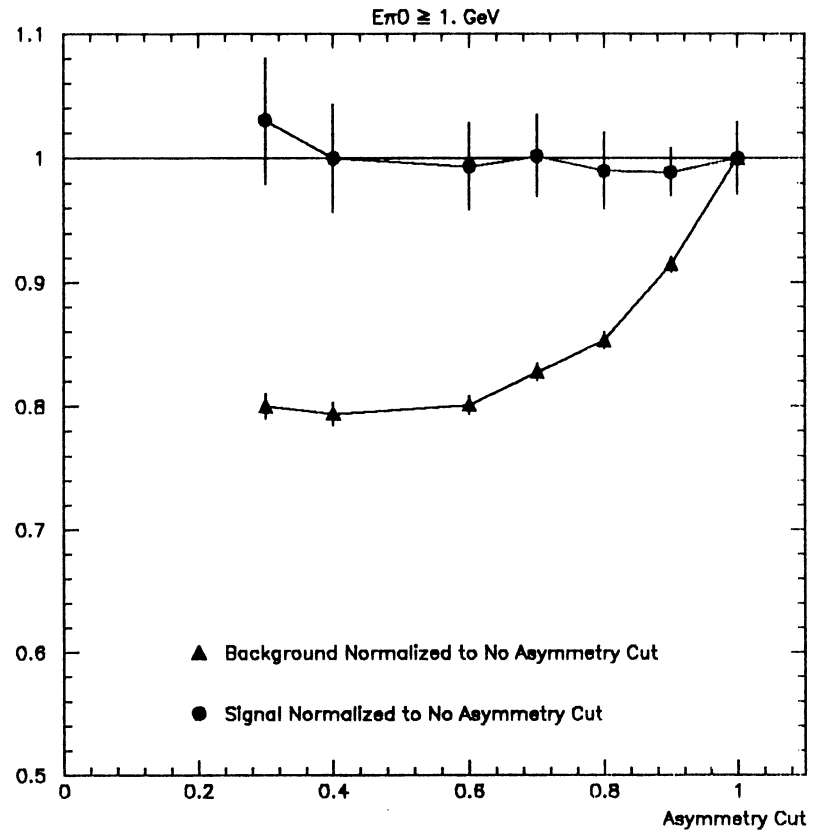

Figure 31: Number of π^0 function of asymmetry cut. Correlations between points not taken into account in the error bars.

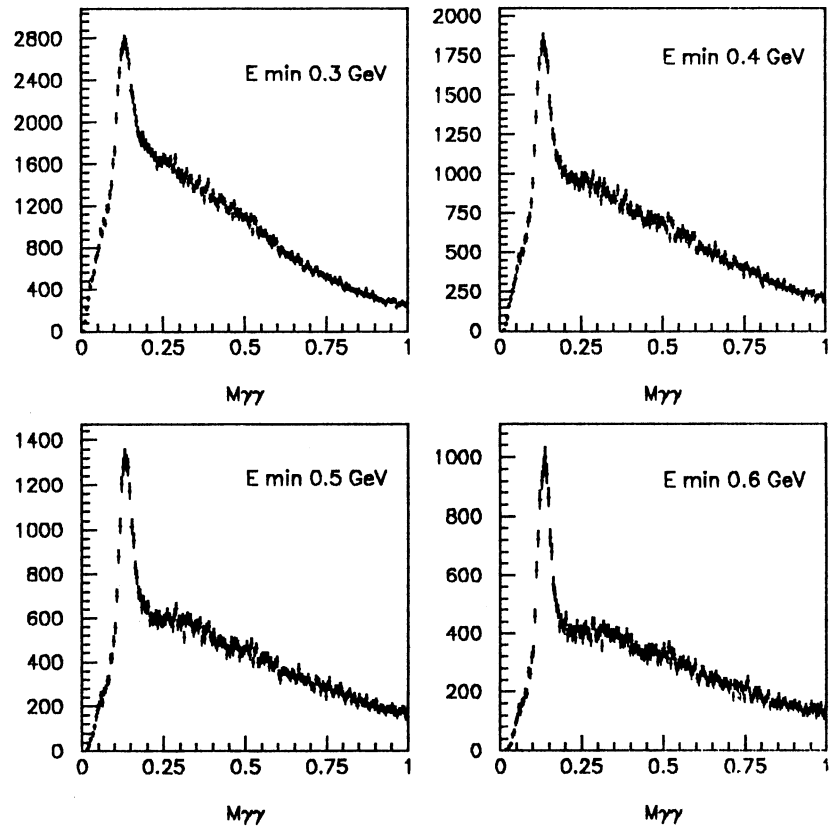

Figure 32: π^0 Mass for different mininum photons energies

Table 3: Number of π^0 function of photon energy cut

E cut (GeV)	Signal	Signal/Backgound	Mass , sigma (MeV)
0.3	11179	0.44	133 , 20
0.4	9307	0.54	134 , 19
0.5	7757	0.70	135 , 19
0.6	5962	0.86	135 , 18

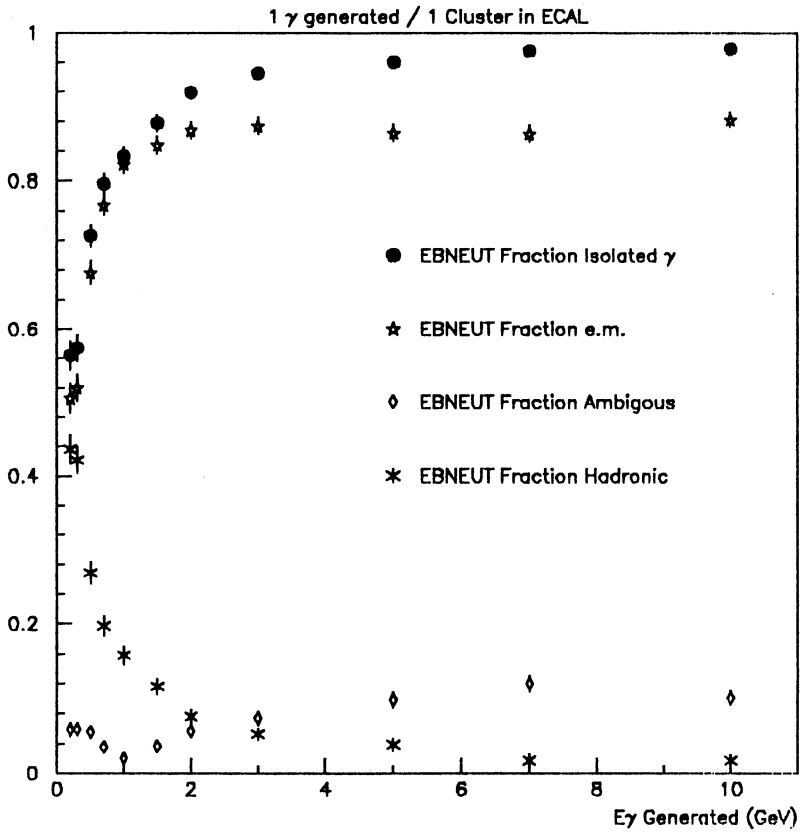

Figure 33: EBNEUT classification on single photons.

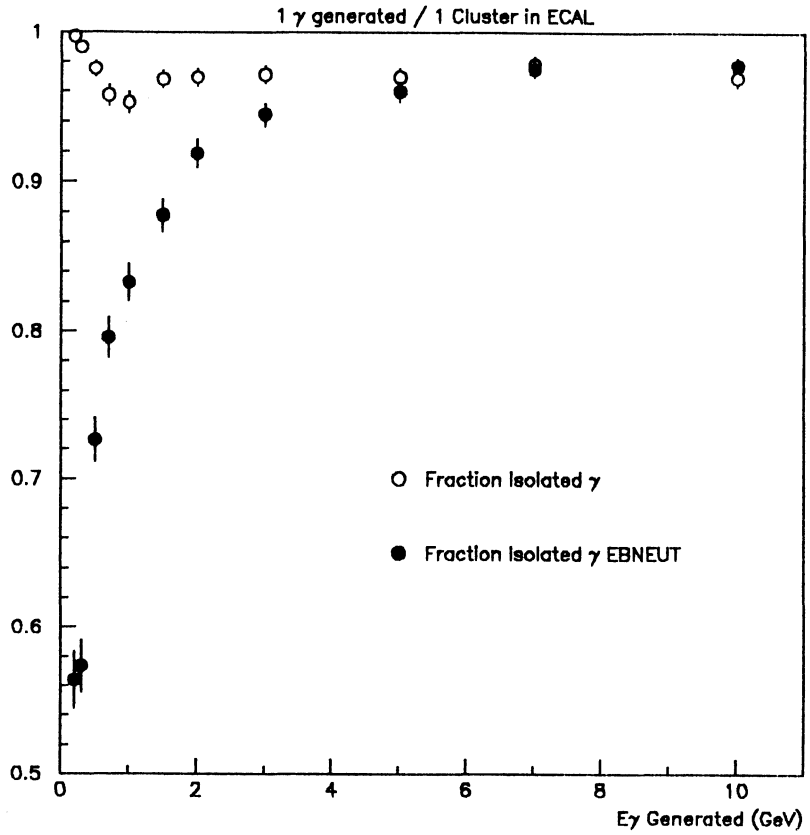

Figure 34: EBNEUT efficiency on Single Photons. Compared to the simple algorithm described in this note.

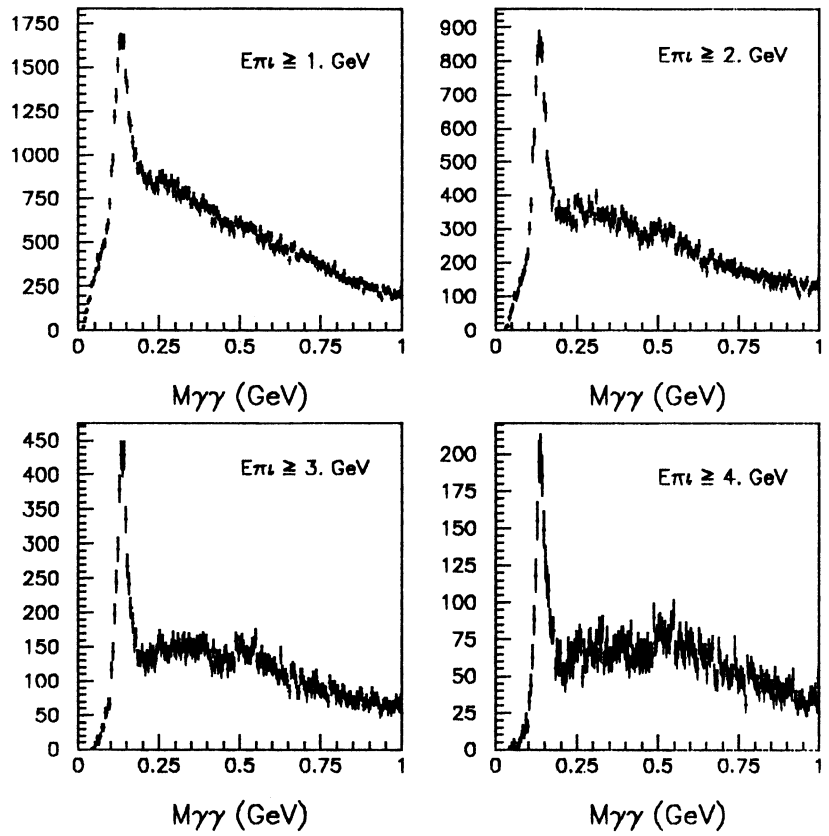

Figure 35: Two photon mass distribution from EBNEUT

Table 4: Number of π^0 from EBNEUT (Data)

E range (GeV)	Signal	Signal/Backgound	Mass , sigma (MeV)
≥ 1	9524	0.57	134 , 20
≥ 2	4964	0.93	135 , 17
≥ 3	2713	1.54	136 , 17
≥ 4	1307	2.07	139 , 18

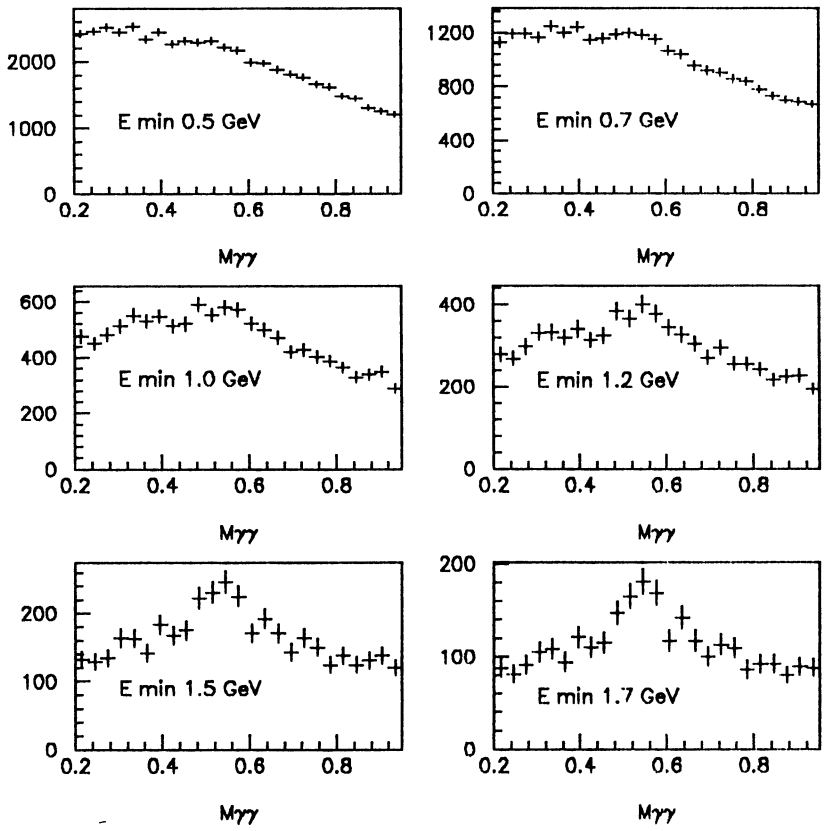

Figure 36: η search: two photon mass distribution. None of the two photons contribute to the π^0 signal.

4. Search for prompt photons in hadronic events.

4.1 Introduction

Prompt photons can be separated from the large amount of non−prompt background because they have a harder energy spectrum and a tendency to be isolated from the hadronic jets.

In the Standard Model, prompt photons in the barrel region come from quark final state radiation (FSR).

It is interesting to study the photons from final state radiation for several reasons. First, since the u−type quarks radiate 4 times as much as the d−type quarks, a measurement of the number of final state photons provides a measurement of the ratio of u−type to d−type quarks in the hadronic event sample, which is related to the couplings of quarks to the Z boson.

Furthermore, a sample of hadronic events with a final state photon is a sample enriched in u−type quarks compared to d−type quarks and, for large enough statistics, such a sample may be useful for various systematic studies. For example, leptons in this sample come mainly from c quarks and they may provide an experimental measurement of the background to b physics. Finally, events with an energetic isolated photon have a topology of charged tracks which is similar to the topology of events with missing energy and they can be used to calibrate some cuts made for Higgs search [4].

Prompt photons in hadronic events are also a signature for new physics (excited quarks, composite models, exotic Higgs, exotic decay of b′,etc...) and it is worthwhile to understand well the final state radiation photons which is the main background for these new processes.

Table 5: Number of FSR photons expected in 30000 hadronic events.

Generator	Process	All photons	5 − 10 GeV	more than 10 GeV
DYMU3	Z to u quarks	2842	251	429
DYMU3	Z to d quarks	760	57	105
BREM5	Z to u quarks	2750	377	521
BREM5	Z to d quarks	840	80	132
JETSET7.2	Z to u quarks	943	86	173
JETSET7.2	Z to d quarks	257	26	30

After some general considerations on final state radiation, the selection of events will be discussed. Then the tools available to reduce the backgrounds (mainly π^0's) will be presented. The background remaining after the cuts will be subtracted using MC. The obtained signal will then be compared to what is expected from final state radiation. A measurement of the ratio of u to d−quarks in Z decays will be described.

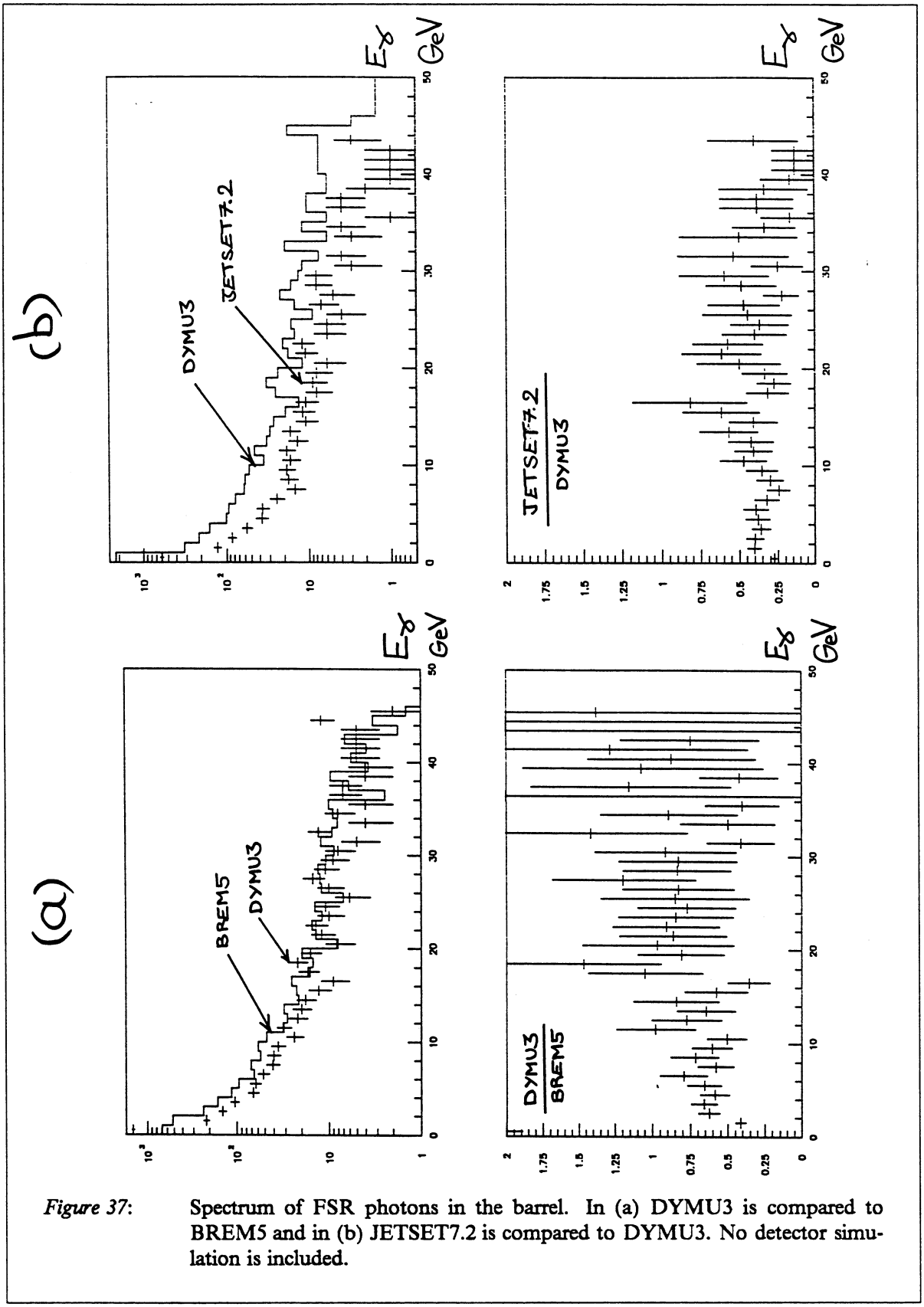

Figure 37: Spectrum of FSR photons in the barrel. In (a) DYMU3 is compared to BREM5 and in (b) JETSET7.2 is compared to DYMU3. No detector simulation is included.

4.2 Theoretical calculation of final state radiation.

Several Monte−Carlo generators include final state photon radiation.

DYMU3 has second order initial state radiation with exponentiation and first order final state radiation with exponentiation. The states produced by DYMU3 contain two quarks and up to 3 photons and are processed through LUND6.3 and HVFL for quark showering, fragmentation and meson decay. DYMU3 is the standard generator of ALEPH for hadronic events and referred to as DYMU02 in the KINGAL library.

BREM5 has first order initial and final state radiation. It is interfaced to LUND6.3 and HVFL like DYMU3.

Version JETSET7.2 of LUND has first order inital and final state photons. In this calculation, the philosophy is different: the final state photons are generated during the showering like quarks and gluons. More than 1 photon can be emitted in the final state. JETSET7.2 is not yet available in KINGAL.

Table 5 on page 40 shows the number of final state photons emitted in the barrel for u and d quarks separately. Taking into account the appropriate fraction of u−type quarks (34% of hadronic Z decays), one gets from DYMU3 that a prompt FSR photon with more than 10 GeV is expected in 0.7% of the hadronic decays of the Z boson.

The rates from DYMU3 and BREM5 are in agreement but the shape of the spectrum is different (Figure 37 on page 41 gives the spectra for DYMU3 and BREM5 as well as the ratio DYMU3/BREM5). The difference at low energy can be understood because BREM5 is first order only. The difference at high energy is more problematic. The rates from JETSET7.2 are 3 times lower than DYMU3 and BREM5 but the spectrum from JETSET7.2 is similar to the spectrum from DYMU3 (Figure 37 on page 41). The origin of these discrepancies is being investigated.

4.3 Preliminary event selection.

In addition to the selection defined in 1.1 on page 1, runs for which the ECAL is considered dubious are rejected: 4530, 4350 (reprocessing problem) 5337, 5385, 5872, 5887, 4017, 4511, 5795, 4384, 5385, 5872 (problem with towers) 5385, 5842, 5872, 5909 (problem with wires).

Hadronic events have to satisfy the following additional cuts :

- The measured vertex of the event has to satisfy : $|z_{vertex}| < 20cm$, $|r_{vertex}| < 10cm$
- $40^0 < \theta_{Thrust} < 140^0$, where the thrust axis has been determined from "good" charged tracks.
- At least 1 neutral PECO cluster in barrel with $E_{corr} \geq 5GeV$.

This selects 18561 events from the POT, and 17669 Monte−Carlo events. The MC production used here is the one defined in 1.1 on page 1.

Some events with a hard isolated photon are displayed on Figure 1 on page i, Figure 38 and Figure 39. The tower energy profile of the photon in event 4981/2242 is shown on Figure 40, giving some feeling of the energy deposition in the ECAL. The interpretation of such impressive events is the main goal in the following.

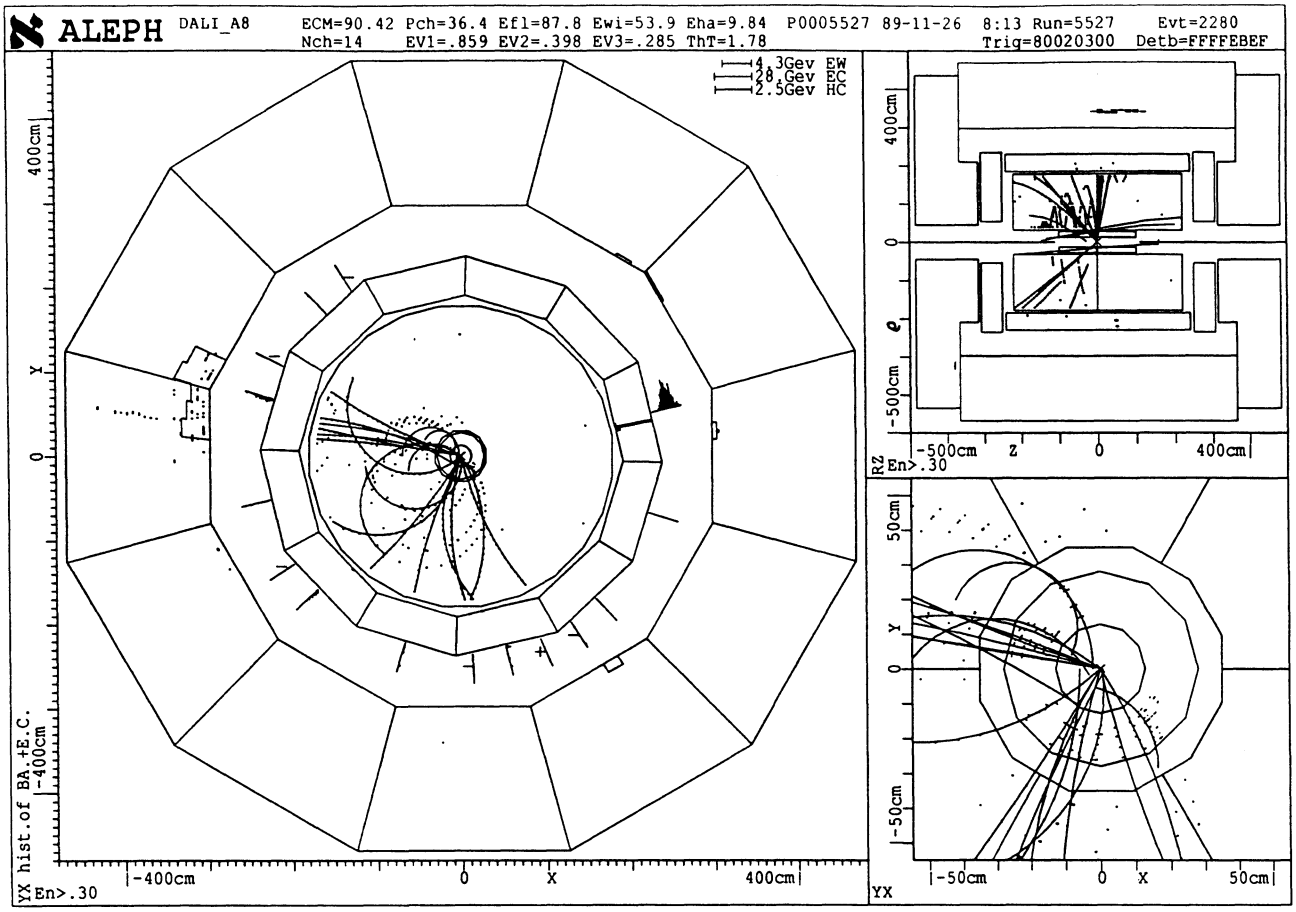

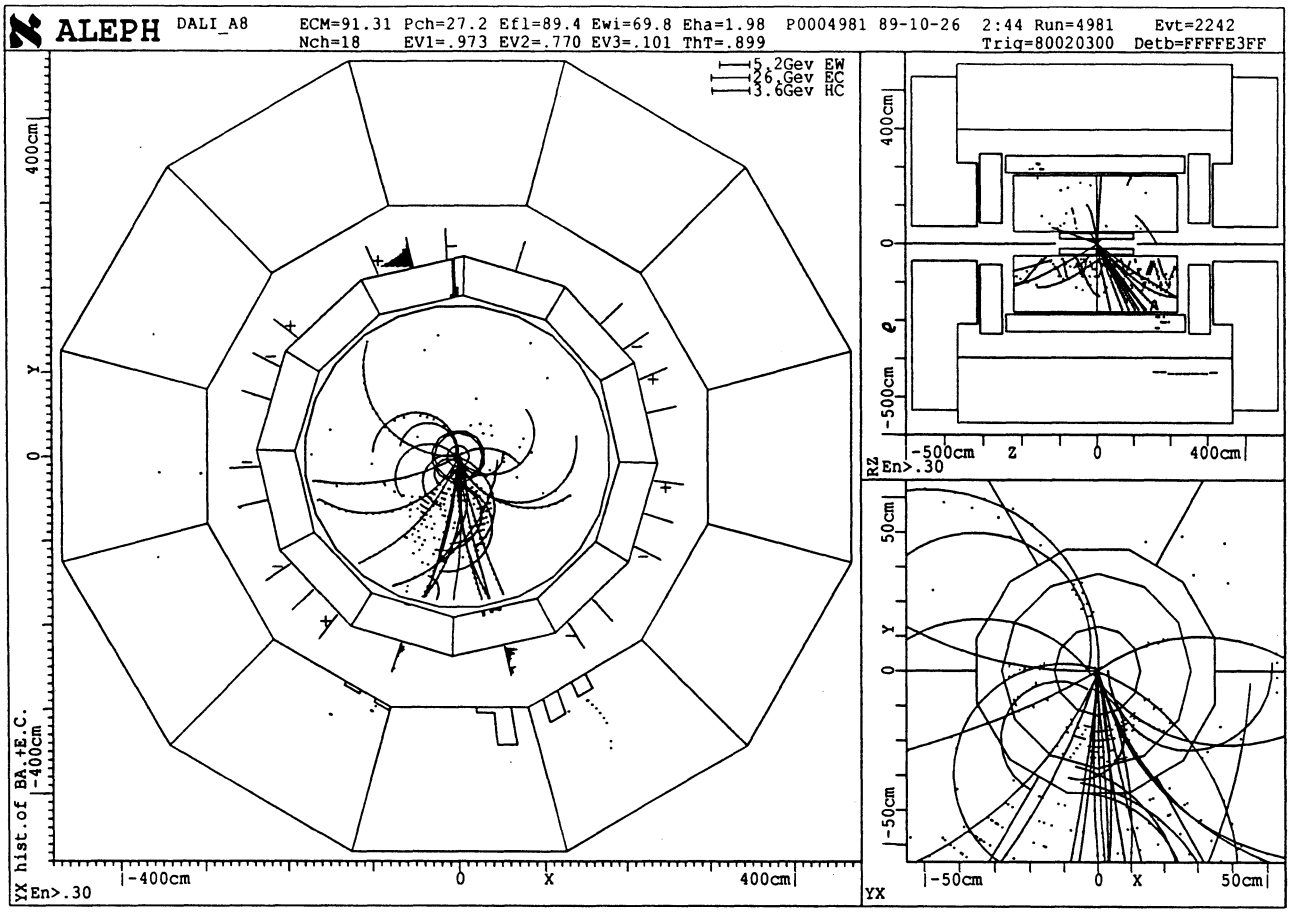

Figure 38: Events with a hard isolated photon (35.8 GeV in event 5527/2280 and 37.4 GeV in event 4981/2242).

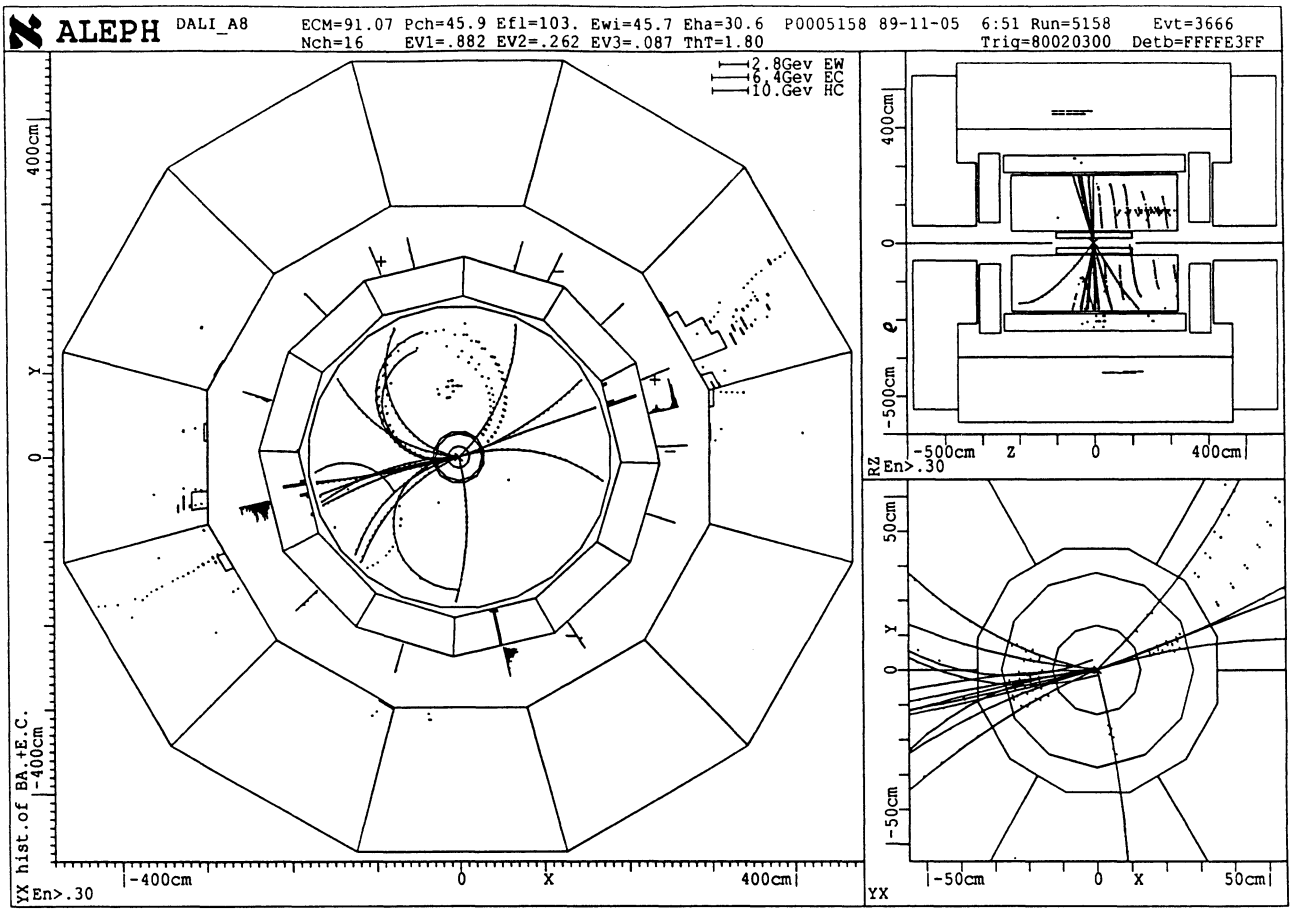

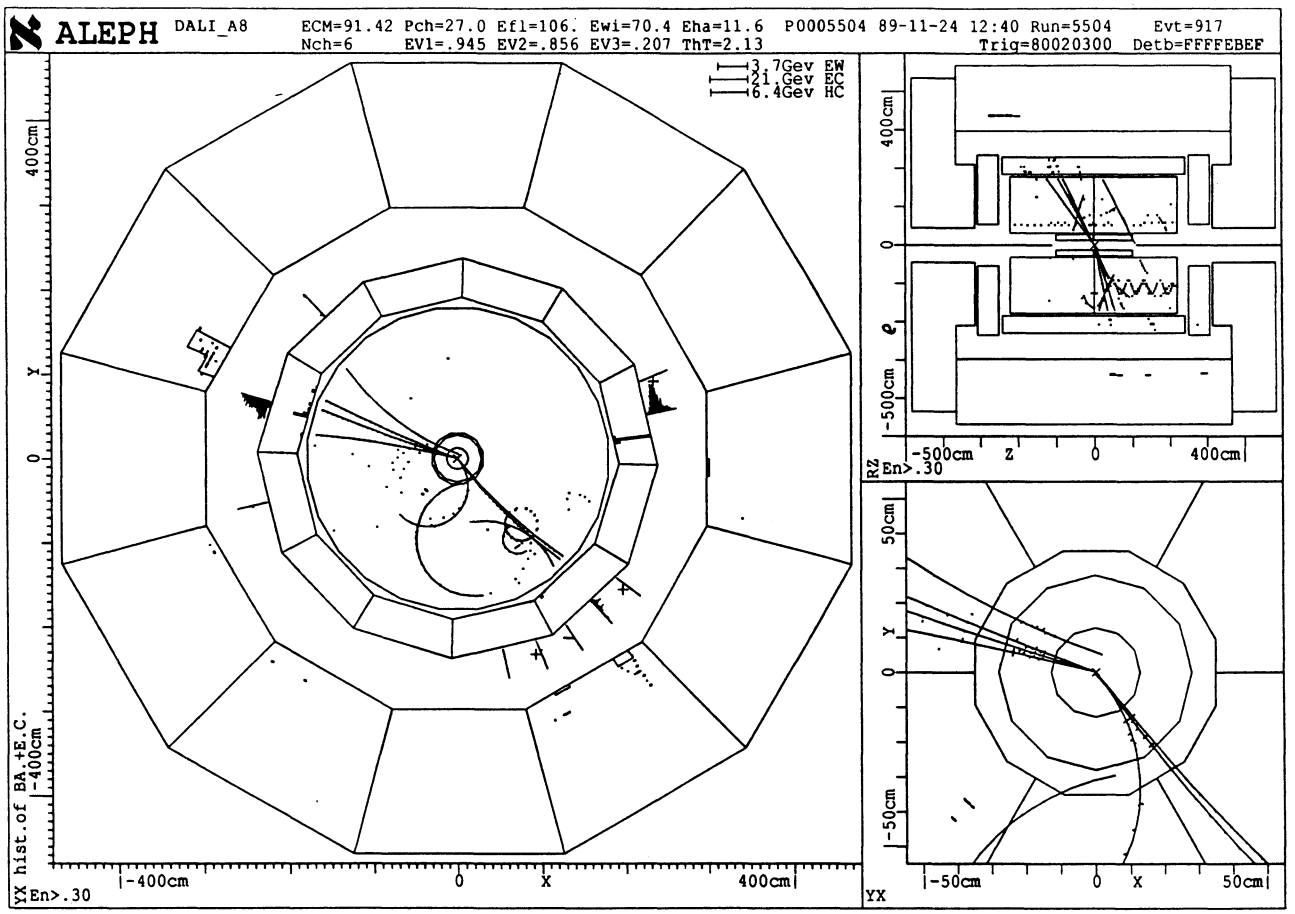

Figure 39: Events with a hard isolated photon (9.5 GeV in event 5158/3666 and 28.7 GeV in event 5504/ 917).

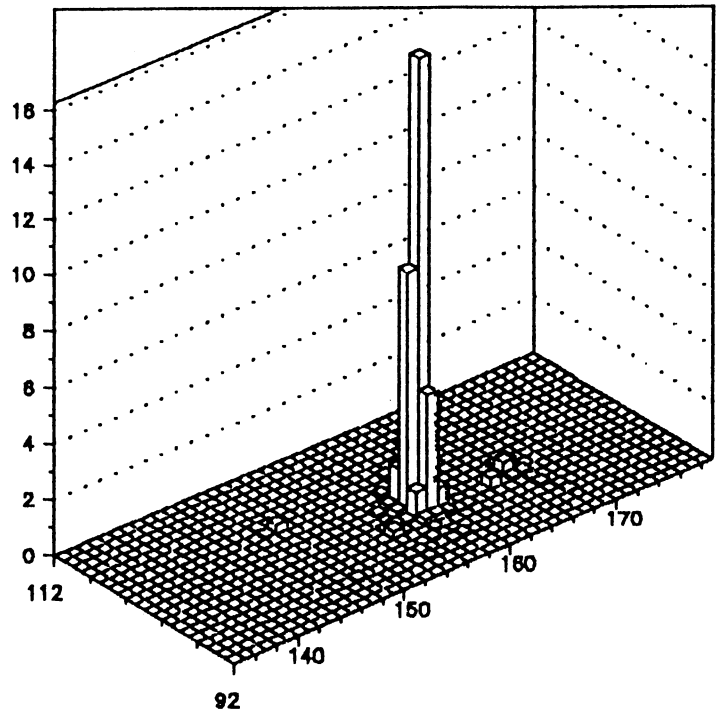

Figure 40: Tower energy profile of the 37.4 GeV photon in event 4981/2242. The vertical scale is in GeV. The horizontal scale refers to the tower number (92 to 111 in ϕ and 135 to 178 in θ).

The selection of hard prompt photons will be now discussed in some detail. The first step is a clean selection of neutral clusters in ECAL.

4.4 Neutral cluster selection

For each event, neutral clusters are selected with the following cuts:

1 – neutral clusters are defined from the relation bits of the JULIA bank PECO. This bank contains a word telling wether the cluster is related with a charged track.

2 – only clusters well contained in the barrel are used ($|\cos\theta| < 0.7$)

3 – The corrected energy has to be in the range : $5 < E_{corr} < 80 GeV$. The 80 GeV cut is there to discard clusters due to a spark or a large fluctuation in the noise.

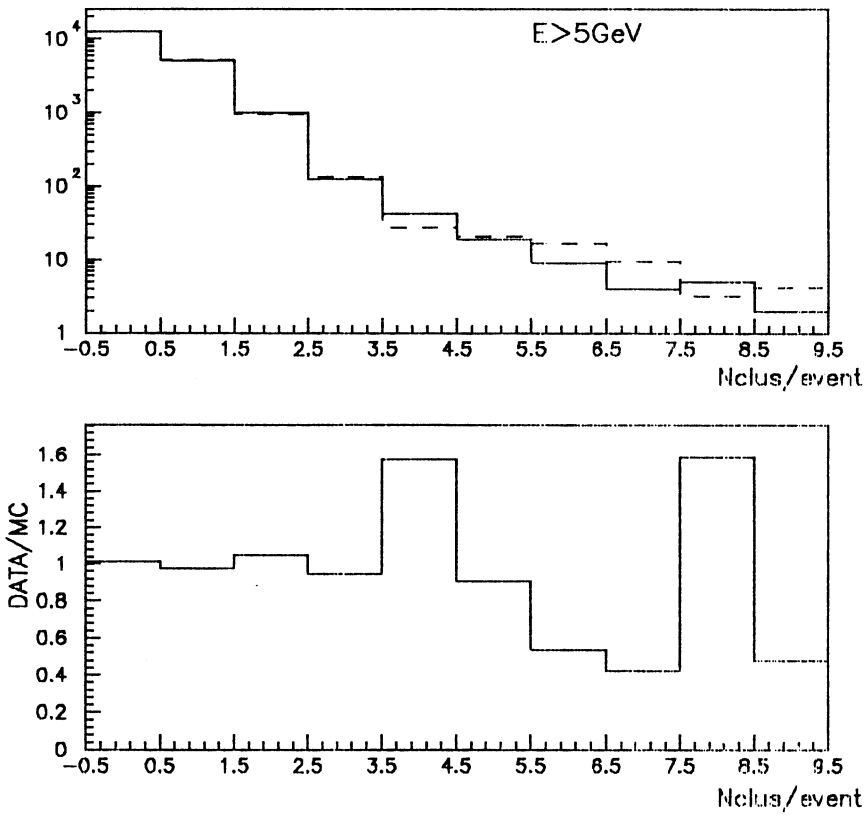

Figure 41: Number of selected clusters satisfying all the neutral cluster selection criteria.

4 – It was found that a number of clusters are due to faulty ECAL electronic front – end cards. These are easily recognizable as a cluster of 16×2 storeys. Sometimes the bad card is surrounded by noise and a simple algorithm has been designed in order to find them (see 2.4.1 on page 8 and subroutine S4CLUS at the end of the note).

5 – In order to select roughly clusters created by photons, a local energy maximum in a 2×2 subcluster is required with an energy $E_{2x2} \geq 2.5 GeV$.

6 – Clusters are rejected when the leading 2×2 tower subcluster has any of its 4 central towers in the edge column of a module (crack) .

7 – The energy of the leading (in terms of energy) tower must be greater than 0.5 GeV (this cut is, in fact, redundant with cut 5).

8 – The fraction of energy in stack3 must be smaller than 0.8 in order to reject plain non electromagnetic garbage.

Figure 41 shows the distribution of the number of selected clusters per event compared to the MC prediction. There is an acceptable agreement between data and MC.

4.5 Selection of isolated prompt photons.

4.5.1 Overview of backgrounds and tools.

The backgrounds for isolated photons are clusters from π^0's and η's, neutral hadrons misidentified as photons and photons radiated by electrons. The background from π^0's dominates.

Using the longitudinal profile of the cluster (variable F_{stk3}), it is easy to reduce the background coming from hadrons.

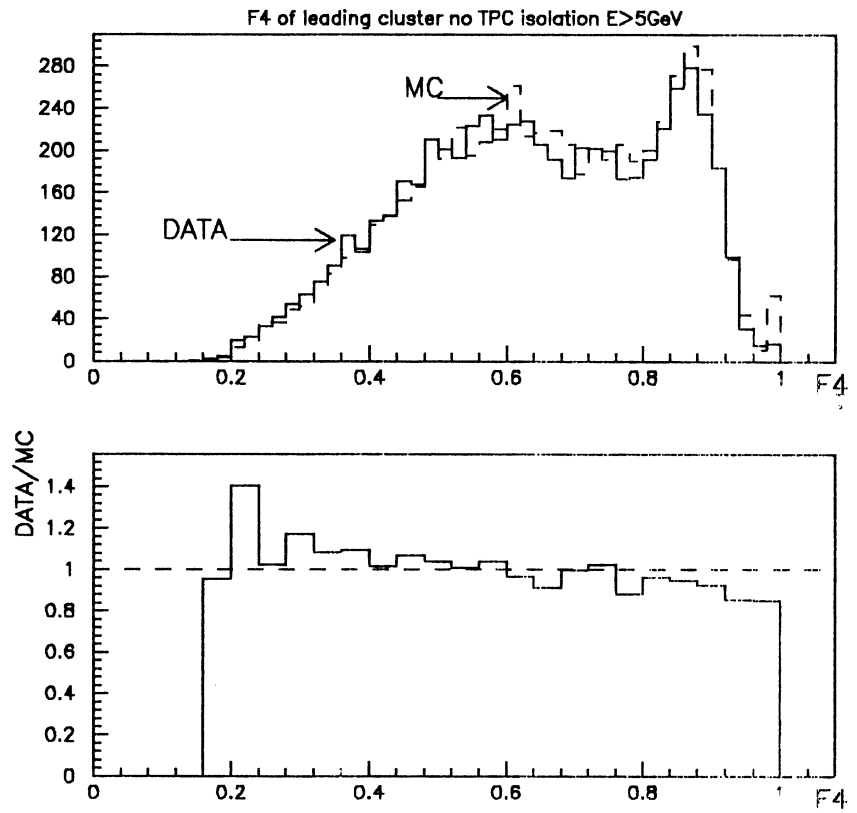

Figure 42: F_4 of the cluster most isolated from charged tracks.

In order to fight against π^0's, the transverse shape of the cluster (variable F_4) will be used. Furthermore, as π^0's tend to be produced within a jet, another useful tool is to require the candidate cluster to be isolated from charged or other neutral tracks.

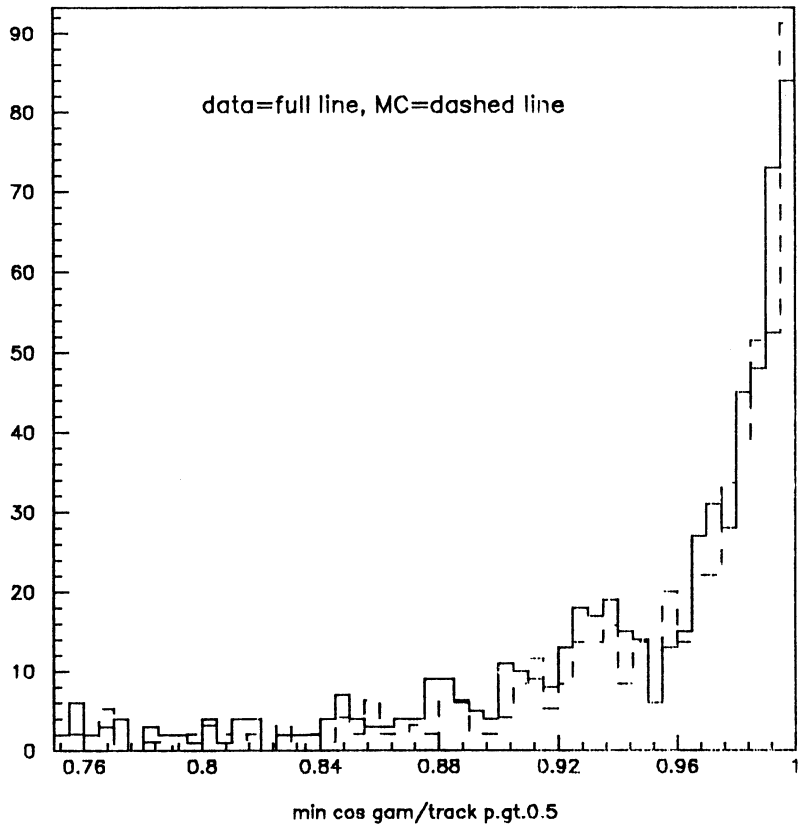

Figure 43: Cosine of the angle. (between the candidate cluster and the nearest charged track with p > 0.5 GeV).

In the following, we will start making minimal cuts and describe problems as they show up. Then more stringent cuts will be made to define a signal.

4.5.2 Isolation from charged tracks.

A loose definition of the isolation will be used first: for each neutral cluster the angle to the nearest "good" reconstructed charged track (see above description) with momentum $\geq p_{cut}$ is computed. For each event, the most isolated cluster in angle defines the isolated photon *candidate*.

Figure 42 on page 47 shows the distribution of F_4 for these clusters ($p_{cut} \geq 0.5 GeV$).[2] The MC does not reproduce the distribution of F_4, as it has already been noticed before (2.4.2 on page 10). There is a deficit of events at low F_4 in the MC. Because of this discrepancy, any cut on F_4 to select clean photons may introduce a bias between the data and the MC.

---

[2] Here F_4 is defined by $\frac{E_4}{E_{raw}}$

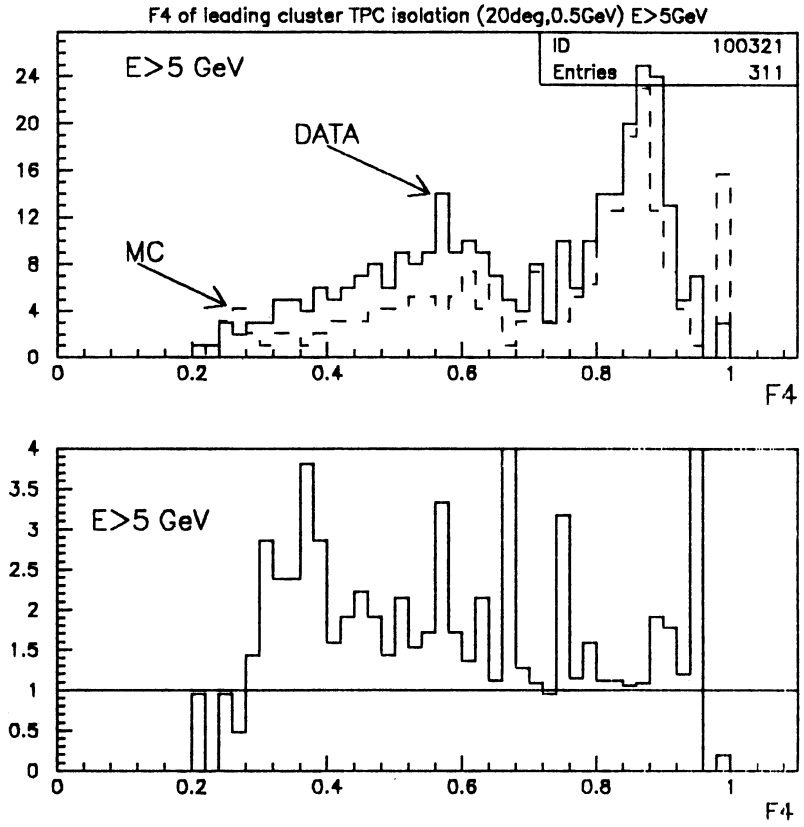

Figure 44: F_4 of cluster isolated from charged tracks $E_{corr} \geq 5GeV, p_{cut} = 0.5GeV, \theta_{cut} = 20^0$

There is also an excess of events in the MC with $F_4 = 1$. This excess can be understood. Using bank PEMH, which relates a cluster with its MC history, this excess is attributed to clusters created by charged particles originated at the main vertex (most of the time this bank is reliable, although it sometimes relates a track at 180 degrees with the cluster in question!). These particles have a well reconstructed TPC/ITC track, but have the peculiarity to deposit more than 5GeV in 1 storey! This is probably a GHEISHA inadequacy. However it should be investigated why JULIA does not associate these clusters with the charged track.

Because the transverse shapes of photons in data and MC are not the same, one would like to rely more on the isolation to reject the background. In the following, it will be required in addition that the cluster is electromagnetic ($F_{stk3} < 0.4$).

Figure 43 on page 48 shows the distribution of the cosine of the angle between the candidate cluster and the nearest "good" charged track of momentum $\geq 0.5GeV$. An isolation cone is defined by 2 parameters: θ_{cut} is the angle to the nearest good charged track of momentum greater than P_{cut}.

The distribution of F_4 for clusters isolated from charged tracks with $\theta_{cut} = 20^0$ and $p_{cut} = 500MeV/c$ is shown in Figure 44 and compared with the MC prediction: there is an excess of data especially at low values of F_4 where π^0's dominate. Figure 45 on page 47 shows the same distribution for

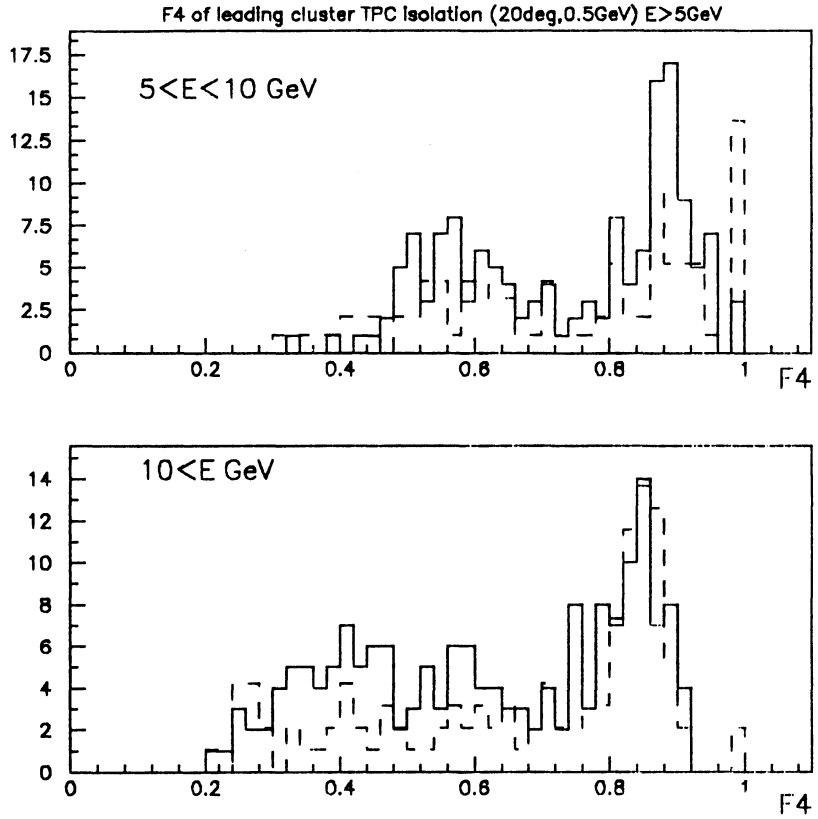

Figure 45: F_4 of cluster isolated from charged tracks $p_{cut} = 0.5GeV, \theta_{cut} = 20^0$

Table 6: Isolation from charged tracks.

The numbers are for clusters above 5 GeV and above 10 GeV in parenthesis.

Pcut, θcut	**DATA**	**MC**	**S/B**
0.2 GeV, 20°	270 (151)	197 (113)	0.5 (0.7)
0.5 GeV, 20°	311 (169)	216 (123)	0.4 (0.7)
1.0 GeV, 20°	394 (212)	300 (154)	0.3 (0.6)
0.2 GeV, 32°	122 (77)	85 (58)	1.0 (1.8)
0.5 GeV, 32°	155 (96)	101 (68)	0.8 (1.4)
1.0 GeV, 32°	224 (146)	172 (111)	0.5 (0.7)
0.2 GeV, 60°	34 (28)	32 (25)	1.0 (1.4)
0.5 GeV, 60°	56 (44)	41 (34)	1.0 (1.3)
1.0 GeV, 60°	126 (99)	93 (67)	0.4 (0.5)

$5 < E < 10$GeV and $E > 10$GeV. At low energies, there is a lack of MC at high F_4 and at high energies there is a lack (50%) of MC in the π^0 region (low F_4).

Table 6 on page 50 gives the number of data and MC candidate clusters (normalized to the number of $Q\bar{Q}$) in bins of (θ_{cut}, P_{cut}), as well as the Signal(FSR)/Background(non FSR) ratio obtained from MC. Numbers in parenthesis are for $E_{corr} \geq 10 GeV$.

The signal over background ratio is still ≤ 1. It is therefore interesting to further reduce the background.

4.5.3 Isolation from charged and neutral tracks.

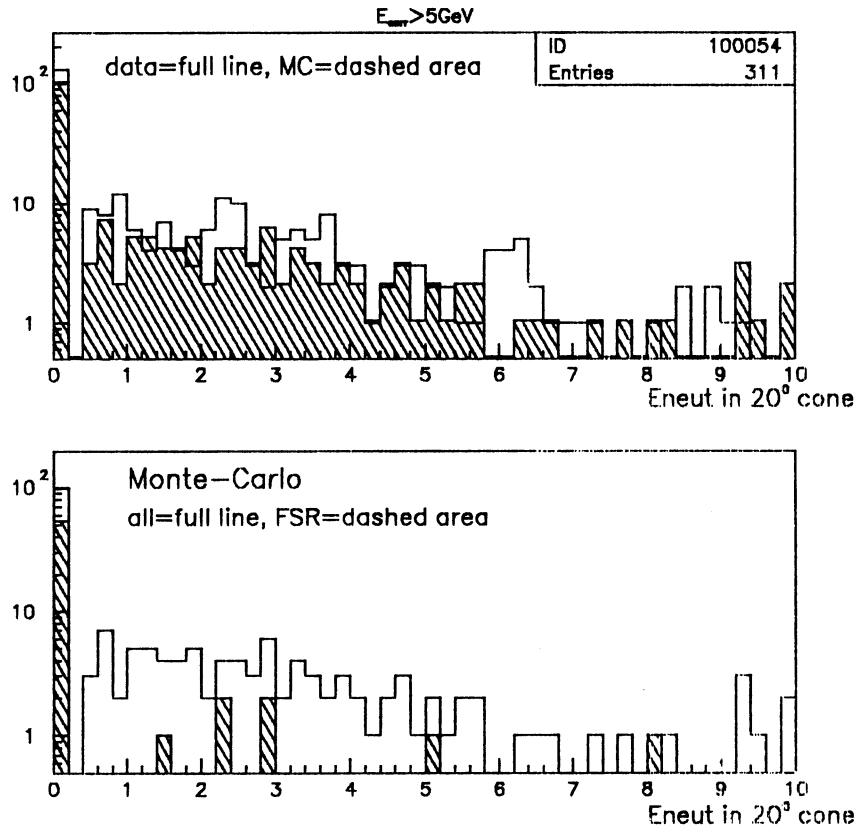

Figure 46: Neutral ECAL energy in 20 degree cone around candidate cluster.

A further reduction in the non FSR background can be obtained by requiring that the candidate cluster be also isolated from neutrals.

Table 7: Isolation from charged and neutral tracks.

Numbers in parenthesis are for E > 10GeV.

Pcut, θcut	DATA	MC	S/B
0.2 GeV, 20°	139 (83)	112 (70)	1.0 (1.7)
0.5 GeV, 20°	160 (93)	116 (71)	1.0 (1.6)
1.0 GeV, 20°	190 (107)	153 (91)	0.7 (1.1)
0.2 GeV, 32°	77 (49)	63 (45)	1.9 (3.8)
0.5 GeV, 32°	97 (60)	67 (48)	1.7 (3.2)
1.0 GeV, 32°	118 (74)	107 (74)	0.9 (1.3)
0.2 GeV, 60°	24 (21)	22 (19)	2.5 (3.5)
0.5 GeV, 60°	35 (30)	28 (25)	2.4 (3.0)
1.0 GeV, 60°	59 (47)	56 (43)	0.8 (1.0)

Figure 46 on page 51 shows the energy sum of the neutral clusters with E > 0.5 GeV in a 20 degree cone around the candidate cluster. In the MC, FSR photons do not have any energy in this cone and with a cut on the sum at 1GeV the S/B is improved by a factor 2 to 2.5, while the loss of signal is 10%.

Figure 47 on page 53 shows the distribution of F_4 for the candidate cluster when charged isolation is applied with $\theta_{cut} = 20^0, p_{cut} = 0.5GeV$, as well as a cut on the neutral energy of 1GeV in the 20° cone. There is still a deficit of π^0's at low F_4 in the MC.

Table 7 corresponds to Table 6 on page 50 with the isolation from neutral tracks applied in addition.

4.5.4 Final cut and number of events with hard isolated photons.

Finally, a cut on the transverse shape of the cluster is made : $0.75 < F_4 < 0.98$.

Final numbers are displayed in Table 8. The Signal/Background ratio is improved by a factor 3 to 4 compared to Table 6 on page 50 and Table 7, while there is no loss of signal.

The energy spectrum after all cuts for an isolation defined by $\theta_{cut} = 20^0, p_{cut} = 0.5GeV$ is shown on Figure 48. A signal for prompt photons emerges clearly above 10 GeV, above some background. The MC is compatible with the data. The transverse energy of the same photons compared to the thrust axis computed using charged tracks only is displayed in Figure 48 as well as the transverse energy compared to the closest jet. The MMCLUS algorithm with $y_{cut} = 0.02$ has been used.

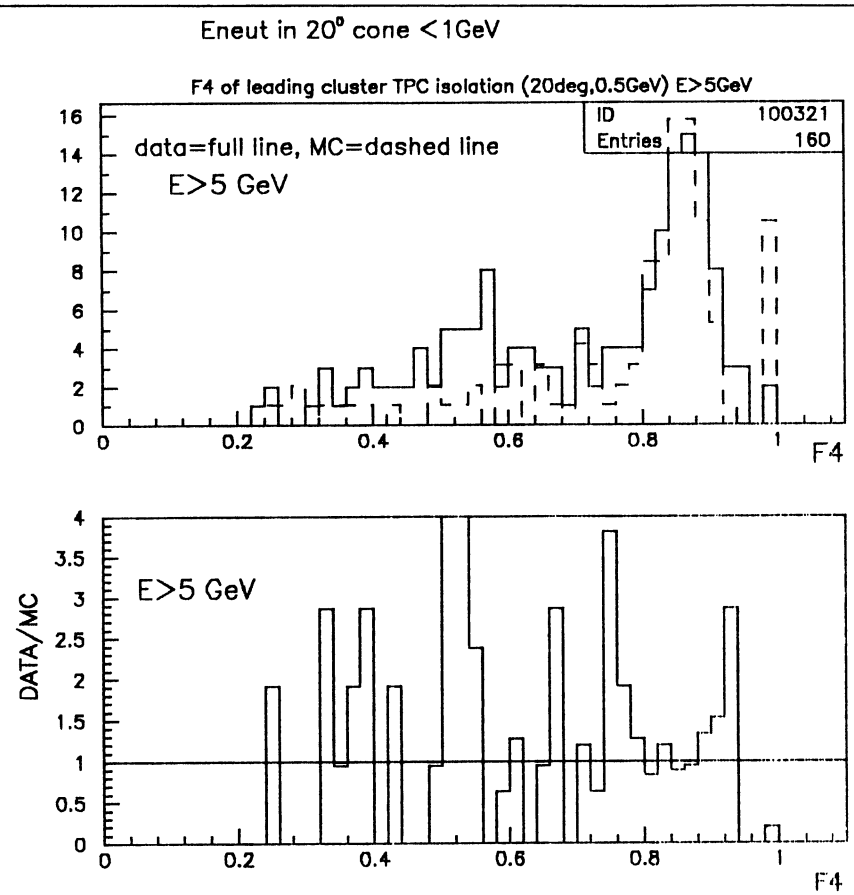

Figure 47: F_4 distribution of candidate clusters with charged isolation ($p_{cut} = 0.5GeV, \theta_{cut} = 20^0$), and neutral isolation (1GeV in 20° cone).

Table 8: Isolation from charged and neutral tracks with F_4 cut.

Numbers in parenthesis are for E > 10GeV.

Pcut, θcut	DATA	MC	S/B
0.2GeV, 20°	76 (45)	70 (50)	3.2 (7.0)
0.5GeV, 20°	85 (50)	71 (50)	3.9 (7.0)
1.0GeV, 20°	94 (54)	85 (59)	3.0 (4.6)
0.2GeV, 32°	49 (29)	46 (38)	7.8 (17.)
0.5GeV, 32°	59 (34)	48 (40)	6.7 (12.)
1.0GeV, 32°	65 (39)	62 (50)	3.9 (5.0)
0.2GeV, 60°	14 (12)	18 (16)	7.5 (14.)
0.5GeV, 60°	20 (16)	23 (21)	6.3 (9.0)
1.0GeV, 60°	26 (20)	30 (26)	3.1 (4.0)

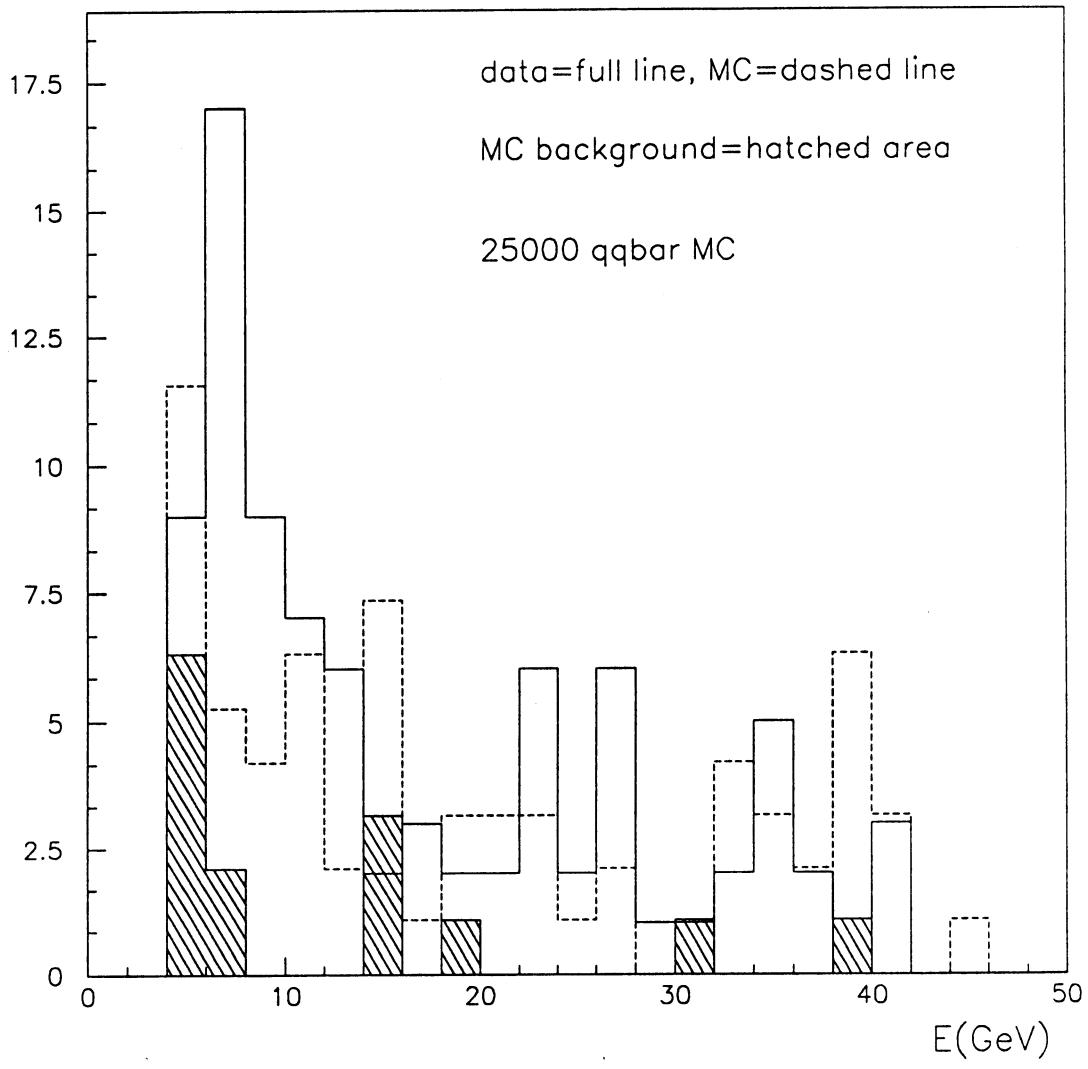

Figure 48: Energy spectrum of prompt photons candidates after all cuts.

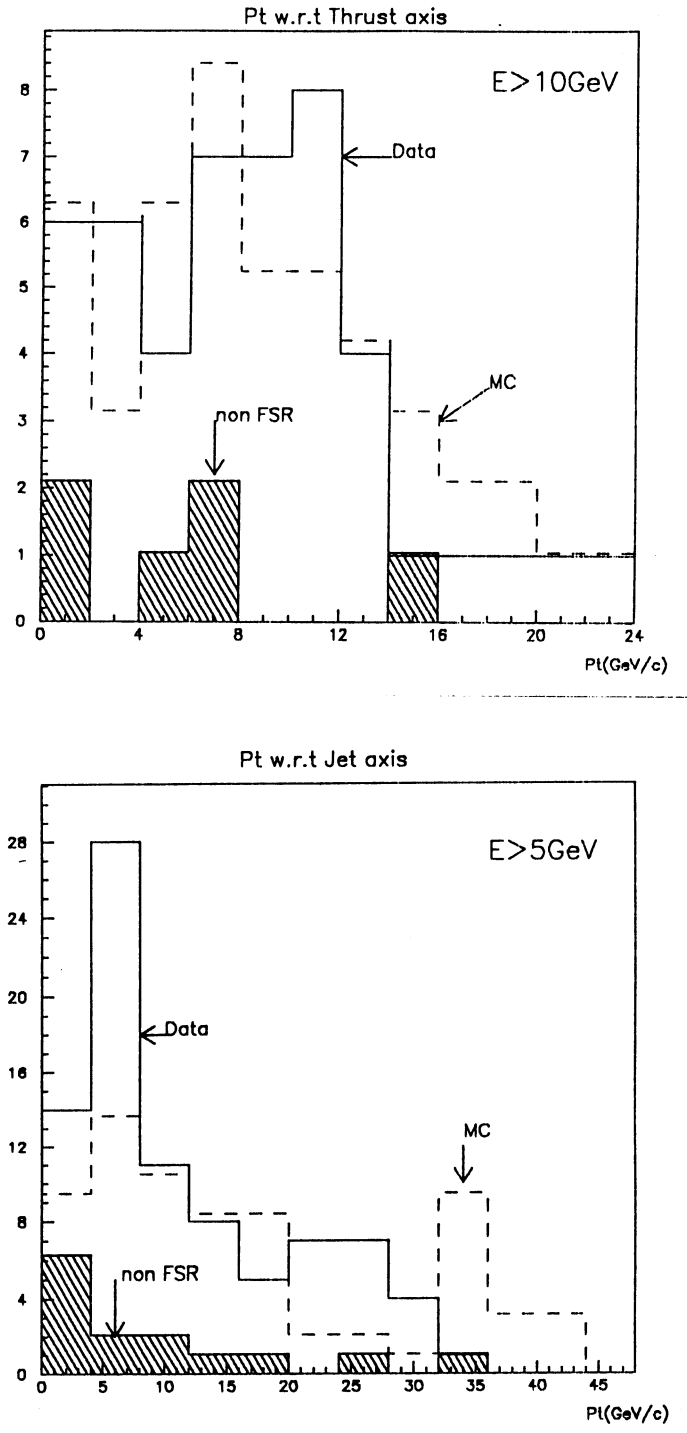

Figure 49: Transverse energy compared to the thrust axis. (computed using charged tracks) of the prompt photon candidates after all cuts and transverse energy compared to the closest jet

4.6 Background subtraction and number of prompt photons.

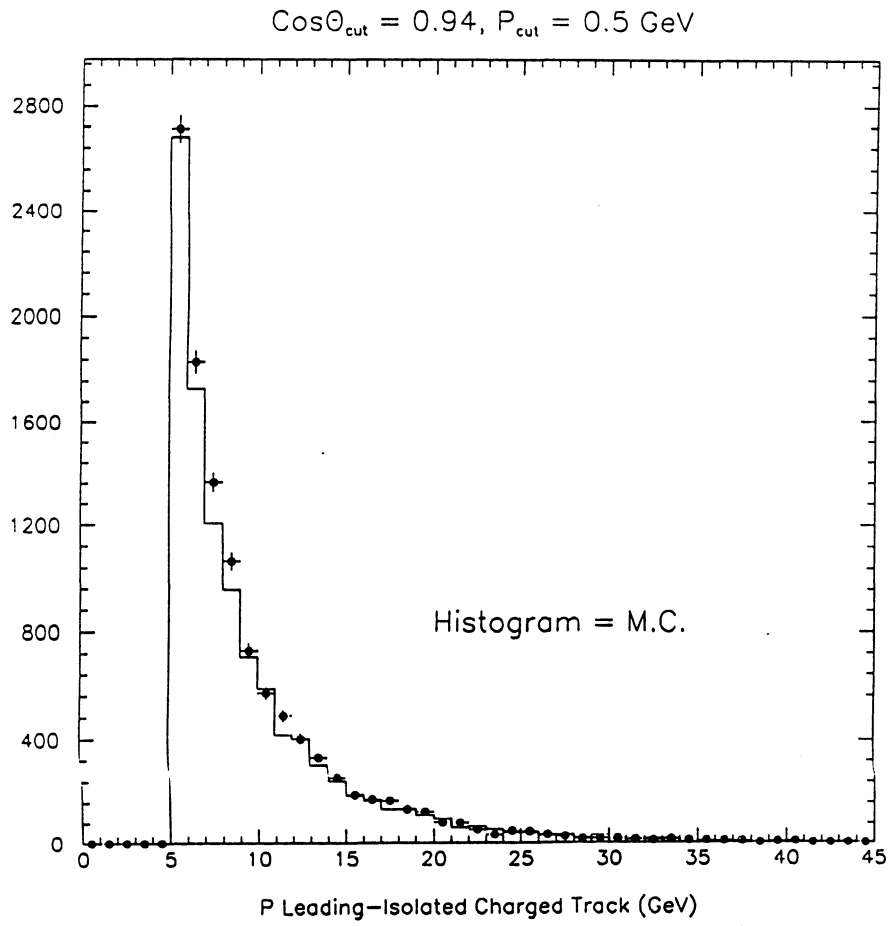

Figure 50: Momentum spectrum of isolated charged tracks. ($p_{cut} = 0.5 GeV/c, \theta_{cut} = 20^0$)

4.6.1 Background subtraction

The remaining background will be subtracted using the MC.

However, there is a substantial disagreement between data and MC. If we do not apply the cut on F_4 (Table 6 on page 50 and Table 7 on page 52), data are in excess of MC of 35% in average. When the cut on F_4 is applied (Table 8 on page 53), this excess disapears or is even reversed for $E \geq 10 GeV$. This is related to the misbehaviour of the transverse shape of the clusters discussed before.

The origin of this problem can be explained by a shift of events from high F_4 to low F_4 in the data. Such a shift can be produced by noise in the detector, causing several nearby clusters to be merged into one single fat cluster or a good cluster being merged with nearby noise. It has been shown before that this effect exists.

Table 9: Numbers of prompt photons after background subtraction.

Numbers in parenthesis are for E > 10GeV.

Pcut, θcut	DATA	MC non − prompt	DATA − background	MC prompt (FSR)
0.2GeV, 20°	76(45)	14(6)	62(39)	56(44)
0.5GeV, 20°	85(50)	15(6)	70(44)	56(44)
1.0GeV, 20°	94(54)	21(11)	73(43)	64(48)
0.2GeV, 32°	49(29)	5(2)	44(27)	41(36)
0.5GeV, 32°	59(34)	6(3)	53(31)	42(37)
1.0GeV, 32°	65(39)	13(8)	52(31)	49(42)
0.2GeV, 60°	14(12)	2(1)	12(11)	16(15)
0.5GeV, 60°	20(16)	3(2)	17(14)	20(19)
1.0GeV, 60°	26(20)	7(5)	19(15)	23(21)

Table 10: Numbers of prompt photons after all cuts.

The background subtraction is done normalising to the observed number of events with $F_4 < 0.75$ (background region = B). The signal region (S) is $0.75 < F_4 < 0.98$. MC considered here is non − prompt only. Numbers in parenthesis are for E > 10GeV.

Pcut, θcut	DATA S	DATA B	MC S	MC B	DATA prompt
0.2GeV, 20°	76(45)	61(38)	14(6)	33(19)	50(33)
0.5GeV, 20°	85(50)	73(43)	15(6)	35(20)	54(37) ~~35(20)~~
1.0GeV, 20°	94(54)	93(53)	21(11)	58(33)	60(36)
0.2GeV, 32°	49(29)	26(20)	5(2)	13(7)	39(21)
0.5GeV, 32°	59(34)	36(26)	6(3)	15(8)	45(24)
1.0GeV, 32°	65(39)	50(35)	13(8)	38(22)	48(26)
0.2GeV, 60°	14(12)	10(9)	2(1)	4(3)	9(9)
0.5GeV, 60°	20(16)	15(14)	3(2)	5(4)	11(9)
1.0GeV, 60°	26(20)	33(27)	7(5)	24(17)	16(12)

Furthermore, the number of isolated π^0's might be wrong in the MC. One way to check this is to look at isolated charged tracks.

Figure 50 on page 56 shows the momentum spectrum of the leading isolated track having an angle to the nearest track with $p_{cut} > 0.5$GeV is greater than 20°. There is a visible 10% excess of isolated charged tracks in the data compared to the MC.

This last test proves that the understanding of isolated tracks, which corresponds to tails in the fragmentation, is not perfect in the MC. The simulation of isolated π^0's suffers probably from the same problem. This effect contributes probably to the bad description of the F_4 distribution for neutral

clusters, in addition to detector simulation problems and inadequacy of the clustering.

It is however difficult to draw a final conclusion about the origin of the problem. Pending better knowledge, the inadequacy of the MC will be taken into account as a systematic error.

Table 9 on page 57 gives the number of data events for the various isolation bins as well as the number of MC events, separating the prompt and the non−prompt contributions.

The background subtraction amounts to 18% for an isolation cone of 20° and 10% for isolation cones of 32° and 60°. One can see that for one given angle, the numbers after background subtraction do not depend strongly on the momentum cut.

The signal of prompt photons is compatible with the expectation from final state radiation for all isolation.

In order to give a final result, the isolation given by $\theta_{cut} = 20^0, p_{cut} = 0.5 GeV$ will be chosen and the result reads:

```
Number of prompt photons E >  5 GeV =  70 ± 10 (stat.)

Number of prompt photons E > 10 GeV =  44 ±  8 (stat.)
```

4.6.2 Systematic error on the background subtraction.

Another method to subtract the background is to use the data themselves. The MC is then used only for extrapolation.

More precisely, it is assumed that the region $F_4 < 0.75$ contains only background. (This is true for the MC but it may be incorrect for the data.) The number of background events that will be subtracted is then the number predicted by the MC in the signal region ($0.75 < F_4 < 0.98$) normalised to the number of events observed in the background region ($F_4 < 0.75$).

The numbers of prompt photons after this background subtraction is given in Table 10 on page 57). Compared to Table 9 on page 57), the numbers of prompt photons are smaller because of the MC deficit in the background region.

For $\theta_{cut} = 20^0, p_{cut} = 0.5 GeV$ the prompt signal is now :

```
Number of prompt photons E >  5 GeV =  54 ± 14 (stat.)

Number of prompt photons E > 10 GeV =  37 ± 10 (stat.)
```

In doing this extrapolation into the signal region, we have assumed that the energy spectrum of isolated π^0's is the same in the data and in the MC, only the overall rate is supposed different. One may get an idea of the rightness of this assumption by comparing the energy spectra of clusters with $F_4 < 0.75$ in the data and MC. Within statistics, the shape of the spectrum agrees with MC (Figure

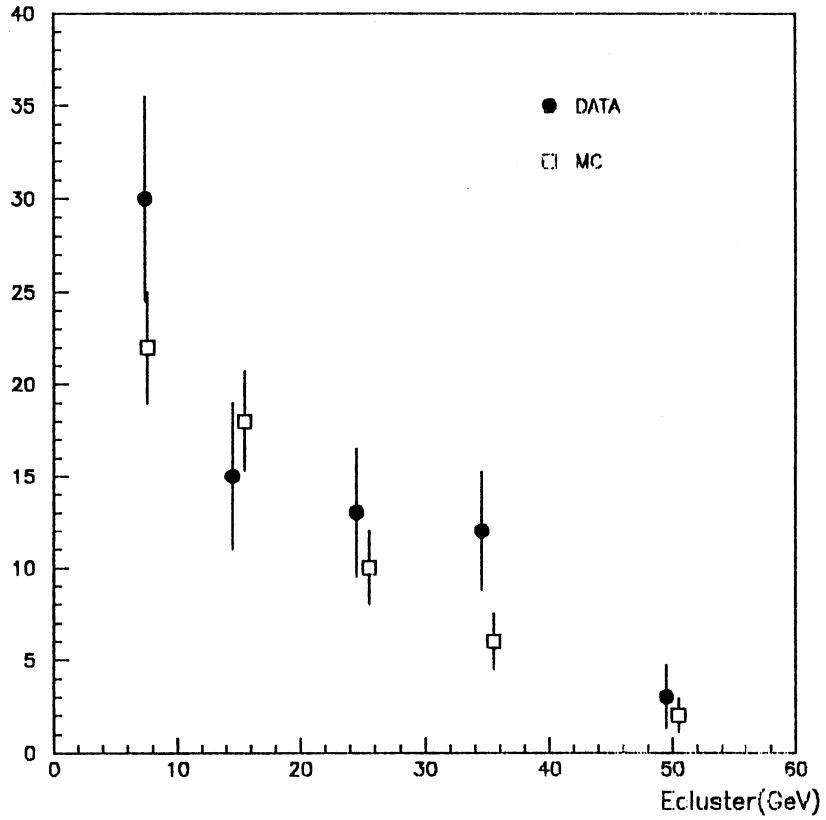

Figure 51: Energy spectrum of clusters in the background region $F_4 < 0.75$.

51).

4.6.3 Systematic error from the photon selection.

The EBNEUT package was also tried as an alternative to select photons. The numbers agree within ± 1 with the numbers obtained with our simple method.

4.6.4 Final result for prompt photons.

The first method is chosen to define the final numbers. The difference between the two methods for the background subtraction sets the systematic error:

Prompt photons E > 5 GeV = 70 ± 10 (stat.) ± 16 (syst.)

Prompt photons E > 10 GeV = 44 ± 8 (stat.) ± 20 (syst.)

This is to be compared to the number of events expected from final state radiation (DYMU3):

```
MC prediction for FSR photons E >  5 GeV =  56 ±  7 (stat.)

MC prediction for FSR photons E > 10 GeV =  44 ±  7 (stat.)
```

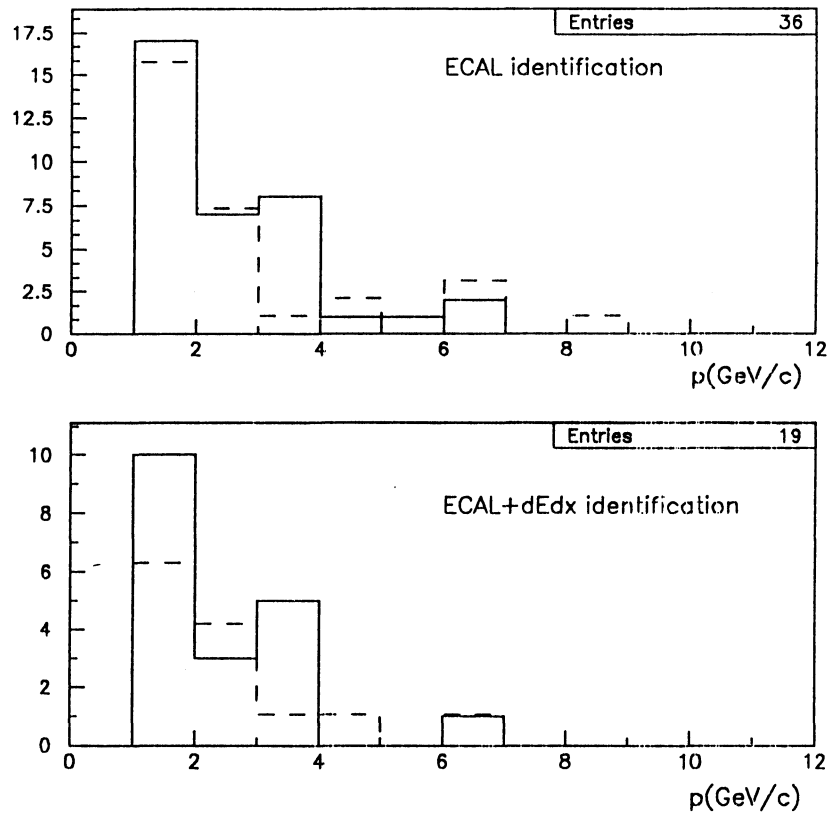

Figure 52: Momentum spectrum of electrons in events containing a hard isolated photon.

Whithin the errors, the measured number of prompt photons is compatible with the expectation from final state radiation from quarks. No new physics is needed to explain these data.

4.7 Analysis of the final state photon sample.

4.7.1 Inclusive lepton spectrum.

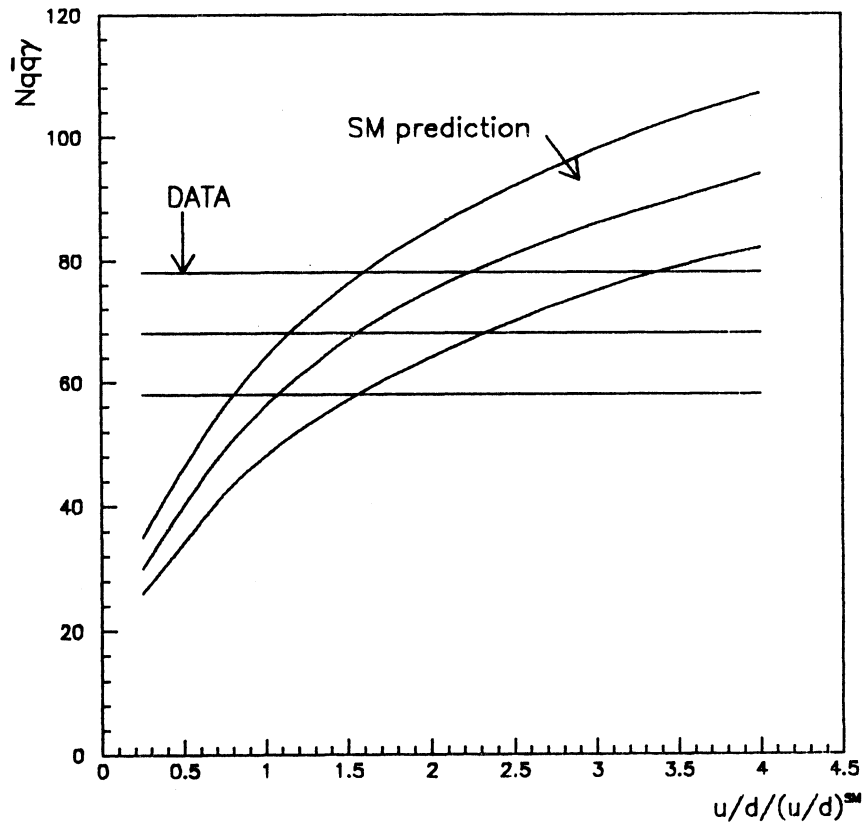

Figure 53: Number of prompt photon candidates from FSR with E > 5GeV as a function of u/d.

The sample of events with a photon from final state radiation is enriched in u−type quarks. Therefore, energetic leptons in this sample come mainly from semileptonic decay of c−quarks. An experimental measurement of these leptons might help understanding the background to b−decays.

The electron identification of the heavy flavors analysis has been used and the spectrum of electrons is given on Figure 52 on page 60. The MC and the data are compatible but the statistics is low. This test will be more conclusive with high statistics.

4.7.2 Measurement of the quark couplings.

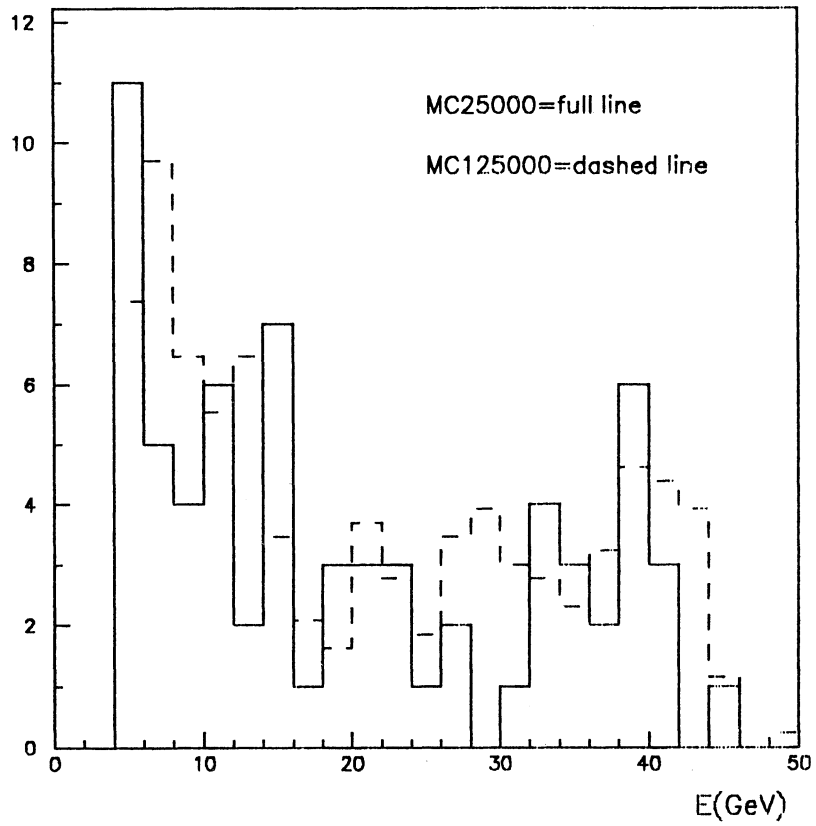

Figure 54: Energy spectrum of prompt photon candidates after cuts for the standard (full line) and the reduced (dashed line) MC production.

4.7.2.1 Principle and result.

The fraction of $Q\bar{Q}$ events with a FSR photon depends on the ratio of up−type quarks over d−type quarks in Z decays. Comparing this fraction with the one predicted for different values of u/d (keeping the total number of hadronic events constant) gives a measure of u/d.

Figure 53 on page 61 shows how the experimental number compares with the MC prediction when u/d is varied. Taking into account the statistics from the data (full lines), as well as from MC (dashed lines), one gets:

$$\frac{u/d}{(u/d)^{SM}} = 1.6\,^{+2.0}_{-0.9}$$

If the MC statistics were infinite, the error bar would become 0.7. If the data statistics were improved by a factor 10 one would get ± 0.2.

This result has a big error from the MC statistics. A dedicated production of MC events through the full chain of KINGAL/GALEPH/JULIA was done after a selection of events at the generation level. This selection requires that the event has at least 1 neutral particle isolated from charged ones

with $p_{cut} = 1GeV, \theta_{cut} = 20^0$ or a photon with more than 20 GeV. This gives a reduction factor of 20 in the number of events to be reconstructed. It is then easy to produce the equivalent of 125000 hadronic events.

Results using this MC production are compatible with the results presented above. The spectrum of photons after cuts is compared to the standard MC production on Figure 54 on page 62.

With the new sample of MC events, the result is :

$$\frac{u/d}{(u/d)^{SM}} = 1.^{+0.7}_{-0.4}$$

4.7.2.2 Systematic error on the quark coupling ratio.

The relative error on $u/d/(u/d)^{SM}$ is about 3 times the relative error on the number of FSR candidates. The following is a list of effects that may participate to a systematic error.

- varying isolation cuts (θ_{cut}, p_{cut}) in ranges shown in Table 8 on page 53, changes u/d by $\pm 20\%$.
- using the second method for the background subtraction reduces u/d by 40% on average over the various isolation bins, in comparison with background subtraction from MC.
- using only charged track isolation (Table 6 on page 50), with $\theta_{cut} = 20^0, p_{cut} = 0.5GeV$, gives

  $u/d/(u/d)^{SM} = 2.7(resp.1.6)$ for $E_{corr} \geq 5GeV$ with MC(resp. data) subtraction of background.

  $u/d/(u/d)^{SM} = 1.0(resp.0.6)$ for $E_{corr} \geq 10GeV$ with MC(resp. data) subtraction of background.
- increasing the cut on E_{corr} to 10GeV, gives

  $$\frac{u/d}{(u/d)^{SM}} = 1.^{+1.1}_{-0.5}$$

A systematic error of $\pm 1.$ is assigned.

4.7.2.3 Final result on the quark couplings :

The final result on the ratio of u to d−type quarks is :

$$\frac{u/d}{(u/d)^{SM}} = 1.^{+0.7}_{-0.4}(stat.) \pm 1.(syst.)$$

This result is compatible with the standard model prediction but suffers from a large statistical and systematical error.

This result can be compared to the result obtained from the heavy flavour semileptonic decays [5]:

6. Acknowledgments

The authors of this report would like to thank W. Atwood, J. Badier, A. Blondel and A. Roussarie for advice and discussions.

Description of routine S4CLUS

```
      SUBROUTINE S4CLUS(ICLUS,E4CLUS,E4ST12,EMAX,CRACK4,IERROR)
C-----------------------------------------------------------------------
C!  - Find Energy in 4 central storeys of a PECO Cluster (in GeV)
C!    bad cards, and the highest energy in 1 tower of the cluster
c!    valid only in BARREL for now!!!
C!
C!   Author    : P.Perez              12-MAR-1990
C!               inspired from E4CLUS
C!
C!   Input :   ICLUS    /I   Row index in PECO Bank
C!
C!   Output:   E4CLUS   /R   energy in 2X2 leading sub cluster
C!             E4ST12   /R   same but only in stacks 1 + 2
C!             EMAX     /R   maximum energy in 1 tower
C!             CRACK4   /L   .true. if one of the towers making the
C!                           2X2 sub cluster is in crack
C!                           (crack= 2 towers from edge of module)
C!             IERROR   /I   0 if OK
C!                          -1 if bad card
C!                          -999 if bad banks
C!
C?
C!=====================================================================
```

References

1. V.P. Marotte, A. Cordier ALEPH 89−164.

2. EBNEUT. J. Badier ALEPH 90−52.

3. Study of the ECAL calibration. E. Monnier ALEPH 89−183.

4. F.Perrier. A calibrated search for $H^0\nu\bar{\nu}$. Presented at the search meeting 20/02/90.

5. Heavy flavour production in Z decays. ALEPH collaboration. CERN EP/90−54.

6. W.B.Atwood and J.Thomas. Observation of the process $e^+e^- \to l^+l^-\gamma$ in ALEPH. ALEPH 90−47.